



HAL
open science

Impacts of highway runoff on metal contamination including rare earth elements in a small urban watershed: case study of Bordeaux Metropole (SW France)

Antoine Lerat-Hardy, Alexandra Coynel, Jörg Schäfer, Antoine Marache, Clément Pereto, Cécile Bossy, Marion-Justine Capdeville, Damien Granger

► To cite this version:

Antoine Lerat-Hardy, Alexandra Coynel, Jörg Schäfer, Antoine Marache, Clément Pereto, et al.. Impacts of highway runoff on metal contamination including rare earth elements in a small urban watershed: case study of Bordeaux Metropole (SW France). Archives of Environmental Contamination and Toxicology, 2021, 193, pp.1-21. 10.1007/s00244-021-00816-4 . hal-03312425

HAL Id: hal-03312425

<https://hal.inrae.fr/hal-03312425>

Submitted on 2 Aug 2021

HAL is a multi-disciplinary open access archive for the deposit and dissemination of scientific research documents, whether they are published or not. The documents may come from teaching and research institutions in France or abroad, or from public or private research centers.

L'archive ouverte pluridisciplinaire **HAL**, est destinée au dépôt et à la diffusion de documents scientifiques de niveau recherche, publiés ou non, émanant des établissements d'enseignement et de recherche français ou étrangers, des laboratoires publics ou privés.



Impacts of Highway Runoff on Metal Contamination Including Rare Earth Elements in a Small Urban Watershed: Case Study of Bordeaux Metropole (SW France)

Antoine Lerat-Hardy¹ · Alexandra Coynel¹ · Jörg Schäfer¹ · Antoine Marache² · Clément Pereto¹ · Cécile Bossy¹ · Marion-Justine Capdeville³ · Damien Granger³

Received: 13 October 2020 / Accepted: 19 January 2021

© The Author(s), under exclusive licence to Springer Science+Business Media, LLC part of Springer Nature 2021

Abstract

High temporal resolution sampling of runoff (15 samples/4 h) and river water (24 samples/24 h) was performed during a major rainstorm (41 mm/4 h) in the Bordeaux Metropole, after a dry and high vehicle-density period. Runoff was sampled at the outlet of one collector draining Northern Bordeaux Highway (NBH; 80,000–93,000 vehicles/day) and river water in the downstream Jalle River. The studied metals, including priority and emergent (Rare Earth Elements [REEs]) contaminants, showed major temporal and spatial variations in the dissolved and particulate concentrations. Hierarchical cluster analyses distinguished metal groups, reflecting different: (i) sources (i.e., automotive traffic: Zn–Cu–Ce and wastewater treatment plant: Cd–Ag–Gd) and/or (ii) processes (i.e., groundwater dilution by rainwater and sorption processes). The contribution of the particulate fraction to total metal fluxes was predominant in the NBH collector (except for Sr and Mo) and highly variable in the Jalle River, where the highest particulate metal loads were due to the export of road dusts exported by the NBH collector. Metal fluxes from the NBH collector represented highly variable fractions of daily fluxes into the Gironde Estuary at the outlet of the Jalle River, depending on elements and partitioning. The resulting relative contributions ranged from: 5% (Sr) to 40% (Cu) for dissolved phases and 30% (As) to 88% (Cu) for particulate phases. The first 40 min of the event accounted for 65% of the suspended particulate matter flux (and associated particulate metals) exported by the NBH collector, whereas the respective water flux contribution was 35%. This finding clearly demonstrates the importance of monitoring the first minutes of rainy events when establishing mass balances in urban systems.

Introduction

Along with increasing world population and urban growth (increasing number of urban agglomerations with more than 1,000,000 inhabitants), cities have sprawled outwards, further and further from city centers, which accentuates the mobility of inhabitants. The insufficient improvement of public transport systems has made private motor vehicles

the most widely used transport mode (Marks 2016). The automotive industry has undergone considerable change in recent years, including safety features and electronic systems, and the development of hybrid and electric cars, etc. (Brauer 2015). Both higher traffic density and technological development require increasing exploitation and use of classic metals, as well as the massive use of different metals with specific properties in new car technology: from a dozen metals in the 1980s to more than 50 metals since the early 2000s (Hocquard 2011). Among these new metals considered as critical for our technological society are Rare Earth Elements (REE; Cobelo-García et al. 2015) composed of lanthanides ($n = 15$), scandium (Sc), and yttrium (Y) (IUPAC 1971).

Traffic-related emissions are concentrated in road dusts (Shi et al. 2010), which are the receptacle for multiple natural and anthropogenic organic and inorganic micropollutants, including metals (Eriksson et al. 2007; Smullen et al. 1999). These road dusts have a high toxicity potential for

✉ Alexandra Coynel
alexandra.coynel@u-bordeaux.fr

¹ Univ. Bordeaux, CNRS, EPOC, EPHE, UMR 5805, 33600 Pessac, France

² University of Bordeaux, CNRS, Arts et Metiers Institute of Technology, Bordeaux INP, INRAE, I2M Bordeaux, 33400 Talence, France

³ SUEZ – Le LyRE, Domaine du Haut-Carré, Bâtiment C4, 43 rue Pierre Noailles, 33405 Talence Cedex, France

aquatic ecosystems when they are transported by runoff waters (Ellis and Revitt 1982; Kayhanian et al. 2008; Yousef et al. 1984). Because most studies reported on selected metals (e.g., Cu, Zn, Cd, Pb, and Ni), limited data are available for other metals (e.g., As, Co, and Sb; Kayhanian 2012; Legret and Pagotto 1999; Wilson 2006). Additionally, new car technology (e.g., introduction of catalytic converters in cars since the mid-1970s) has generated new emissions into environmental compartments, releasing emerging metallic contaminants, such as the Platinum Group Elements (PGE; Schäfer and Puchelt 1998; Wiseman et al. 2016), and a number of other elements, such as REEs (Ce, La, Nd), which are emitted together with PGE from car catalysts (Wiseman et al. 2016). Because the emission of these elements under their application-specific forms is relatively recent, their environmental behavior and fate remain widely undocumented (COST NOTICE-2015).

Urban roads and car parks (industrial and commercial areas) respectively occupy 15% and 46% of the total drained urban area (Bannerman et al. 1993). Metals settled on such urban surfaces during dry periods may tend to be carried away with the early portion of storm runoff causing a first flush of pollutants (Kim et al. 2005, 2006; Lee et al. 2004; Li et al. 2005; Sansalone and Buchberger 1997; Schueler 1987). Because of their limited surface and thus their supposedly low potential contributions (Shelley et al. 1987), urban highways have been less documented in the literature. However, it is essential to characterize runoff from urban highways, because they can carry a large quantity of metals due to their specific characteristics (e.g., safety fences, noise barriers). The stormwater quality from highway leaching/runoff can impact the water quality in receiving water bodies and contribute to river degradation. Sampling strategies addressing the impacts of highway runoff on peri-urban rivers need high temporal resolution monitoring. Because metals are transported either in dissolved phase or in particulate phases of runoff waters and partitioning may change with oxidation–reduction reactions and pH (Ball 2002; Han et al. 2006), there may be rapid changes in speciation with a transition from the particulate phase to the dissolved phase and vice versa (Kayhanian et al. 2007; Lau et al. 2009; Westerglund and Viklander 2006). Unfortunately, not all studies address dissolved and particulate fractions separately, as most studies have focused on the total phase (dissolved plus particulate; Huber et al. 2016). However, partitioning plays a major role in aqueous contaminant transport and dispersion (e.g., sedimentation vs. dilution), and knowledge on metal partitioning is important to determine or optimize the most effective stormwater treatment strategies (Li et al. 2008, 2006; Maniquiz-Redillas and Kim 2014).

Based on a geochemical monitoring on two strategic sites (stormwater collector of highway and outlet of a river) on the urban Jalle River, draining part of the Bordeaux Metropole,

this study was designed to evaluate the impact of highway runoff during a summer rainstorm in September 2016 on the metal transport in a small urban watershed. The main objectives were (i) to analyze temporal variability of the dissolved and particulate trace metals during different periods of the rainy event with a focus on REEs, (ii) to assess trace metal profiles of road dust and other urban metal sources by comparison between both sites, (iii) to evaluate the contribution of the metal fluxes from stormwater collected of highway to those exported by the Jalle River during this major rainy event, focusing on the role of the first flush (<40 min), and (iv) to address the potential of runoff water treatment to limit river pollution.

Materials and Methods

Presentation of the Study Sites and the Sampling Strategy

The Bordeaux urban highway is the longest in France (~45 km), has an average annual daily traffic (AADT) of 250,000 vehicles, and is the second most congested after the Paris urban highway. Indeed, the large number of commuters and the fact that the Bordeaux highway is a major traffic knot in southwest France (holiday region and main axis between France and Spain) cause high motor vehicle densities and frequent traffic congestion. The Bordeaux highway pavement is asphalt surface and speed limit is 90 km h⁻¹ in normal condition. The Bordeaux highway is bordered by “natural” noise barriers made of walls of soil or constructions. Surfaces close to the Bordeaux highway are mainly covered by urban fabric, industrial, and/or commercial zones. Runoff waters from the Bordeaux highway are channeled to stormwater collectors before being discharged into urban rivers tributary to the Gironde Estuary. The Northern Bordeaux Highway (NBH) collector is one of the most important collectors of the Bordeaux highway drainage system, draining ~18.2 km² (Fig. 1) with an AADT comprised between 80,000 and 93,000 vehicles, of which 6.5% are trucks.

The Jalle Watershed covers an area of 330 km², i.e., ~57% of the Bordeaux Metropole area making it the most important tributary of the Garonne Branch of the Gironde Estuary within the Bordeaux agglomeration (Fig. 1). The Jalle River receives the water from (i) a less urbanized upper watershed mainly characterized by agricultural surfaces, (ii) mixed urban areas [e.g., wastewater treatment plant (WWTP) effluents], and (iii) the NBH collector (Fig. 1). In its central part, the Jalle River consists of two main branches; the southern branch receives the WWTP effluents (Fig. 1). The average annual precipitation value for Bordeaux Metropole is 944 mm (1981–2010) (Météo France 2019). The average annual discharge at the outlet

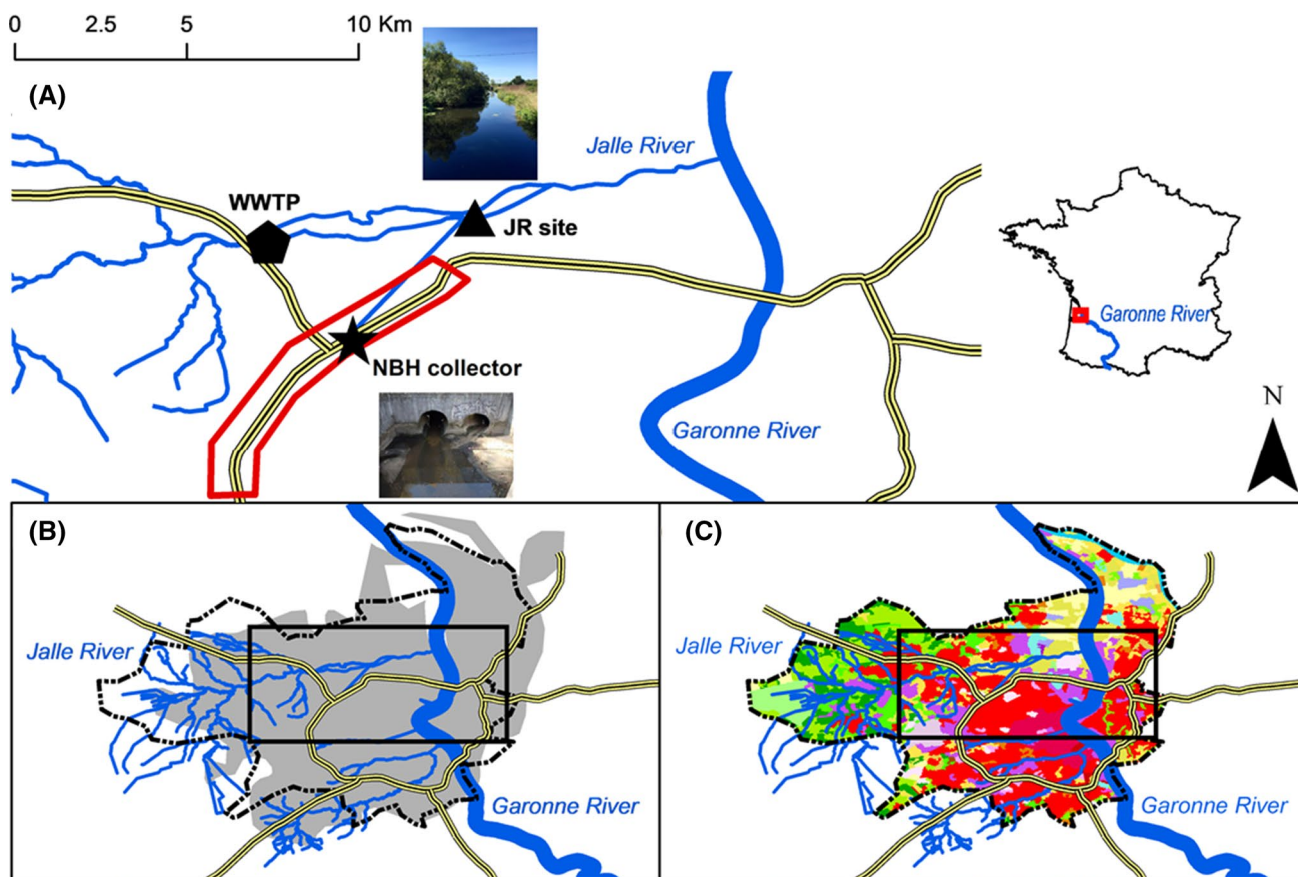


Fig. 1 **a** Location of the sampling sites (NBH collector and JR site) and the WWTP on the Jalle River watershed. The red frame delimits the part of the highway whose runoff water goes to the NBH collector. **b** Presentation of the extent of the urban area of Bordeaux (grey background), the main rivers crossing it, and its highway system (yellow/black line). The administrative boundaries of Bordeaux Metro-

pole are represented by a dotted black line. The black frame delimits the zoom of map A. **c** Presentation of the land use of Bordeaux Metropole. The yellow/green shades represent forest and agricultural surfaces. The red/purple shades represent urbanized surfaces. The black frame delimits the zoom of map A

of the Jalle River is $1.80 \text{ m}^3 \text{ s}^{-1}$ with high temporal variations (e.g., from 0.40 to $44.0 \text{ m}^3 \text{ s}^{-1}$ in 2016–2017). The banks of the Jalle River are mainly vegetated (prairies and forests), including a natural reserve in the downstream part (Fig. 1).

On the night of September 13–14, 2016, an intense rain event (41 mm in ~4 h corresponding to 63% of the monthly precipitation) occurred after 2 months of dry weather with intense road traffic due to summer holidays. Sampling was performed at two sites during the rain event to characterize both runoff waters in the NBH collector and waters transported by the Jalle River downstream near the natural reserve (JR site; Fig. 1). The JR site is located on the southern branch, upstream of the limit of tidal influence (6 km upstream of the confluence with the Garonne Branch of the Gironde Estuary) and integrates the main water masses of the Jalle River watershed, including WWTP and NBH collector effluents.

For the NBH collector site, high-frequency sampling was conducted on September 13, 2016 between 07:30 PM and 11:30 PM (15 samples in 4 h). The sampling intervals gradually increased from 5 min at the beginning of the event (first flush) to 1 h at the end of the event. The samples were taken manually using a clean plastic bucket, previously rinsed with water from the site. From September 13 noon to September 14 noon, parallel hydrogeochemical monitoring was conducted on the Jalle River with hourly sampling (each sample integrating 3 samples every 20 min) during 24 h using previously acid-cleaned bottles in an automatic sampler (SIGMA 900P) on the south river bank. Samples were collected close to the bank (~1 m) in the stream. The discharge of the NBH collector is located 250 m upstream of the sampling point on the Jalle River allowing a good mixing of the two water masses.

Water Discharge, SPM Concentrations, Physical and Chemical Parameters

The discharges at the NBH collector and JR sites were obtained via the Suez research and expertise center, the LyRE (Hydreka® Doppler flowmeters, model “Mainstream,” associated with piezometric sensors). For both sites, Suspended Particulate Matter (SPM) concentrations were determined in the laboratory by filtering a known volume of water through preweighed filters with a porosity of 0.7 µm (glass microfiber, Xilab®). Once dried, the filters were reweighed. The difference between the final weight and the initial weight brought back to the filtered water volume gives the SPM concentration.

For NBH collector site, in situ sampling was performed by the LyRE. The nitrogen concentration (NTK method), dissolved organic carbon concentration (DOC), biological oxygen demand (X5-BOD), and chemical oxygen demand (COD) of the samples were determined in laboratory by the LyRE. At the JR site, probes installed as part of the SIRENE network by the LyRE have recorded the water temperature (Temp), dissolved oxygen concentration (O₂), pH, and conductivity (Cond) every 15 min.

Sample Treatment and Analysis

The samples for dissolved metal analyses were filtered (Sartorius-Minisart®, < 0.2 µm) into previously decontaminated polypropylene bottles, acidified (ultra-pure HNO₃; J.T. Baker®, 14 M) and stored at 4 °C in the dark, pending analysis. Raw water samples for SPM recovery were collected in 6-L containers at NBH collector and in 1-L containers at the JR site. Due to the relatively low SPM concentrations in the Jalle River, the 24-hourly samples were pooled to form four composite samples (covering 7, 3, 6, and 6 h each), in order to obtain enough material to perform the acid digestion, except 2-hourly samples, which were individually digested. Once in the laboratory, the samples were centrifuged in a cooled centrifuge (4000 rpm, Jouan®), and the retrieved SPM were subsequently dried to constant weight at 50 °C in an oven and crushed in an agate mortar. Two different acid digestions of sample aliquots were performed in polypropylene tubes (DigiTUBES®, SCP SCIENCE) using (i) Aqua Regia (5 mL Suprapure HCl 10 M, Merck® and 3 mL Suprapure HNO₃ 14 M, Merck®); and (ii) HCl/HNO₃/HF (1.5 mL Suprapure HCl 10 M, Merck®; 0.75 mL Suprapure HNO₃ 14 M, Merck®; and 2.5 mL Suprapure HF 29 M Fisher®) in a heating block (2 h—110 °C). The complete detailed protocols are described in Abdou et al. (2016) and Gil-Díaz et al. (2018).

Trace elements were analyzed with an Inductively Coupled Plasma Mass Spectrometer (Thermo Scientific® X-SERIES 2 ICP-MS), and REE concentrations were

determined with a Triple Quadrupole Inductively Coupled Plasma Mass Spectrometer (Thermo Scientific® iCAP TQ—ICP-MS). For each element, a calibration line was obtained using known standard solutions. For REE concentrations, Triple Quadrupole (TQ) mode, with dioxygen as the reagent gas (O₂), was preferred to eliminate as many interferences as possible. In addition, for REEs, single-element solutions were analyzed for each potential interferent to correct each sample. The corrections applied are less than 8%. The analytical methodology for REEs is detailed more specifically in Lerat-Hardy et al. (2019).

Analytical quality monitoring was performed by measuring certified reference water and sediments. The accuracy and precision of the analyses are shown in Table 1. For CRM water (NRC SLRS-6), the results showed average recoveries of 91% with typical precision of 9% RSD for all REEs and for all other trace metals recoveries averaged 96% with mean a precision of 8% RSD (Supplementary Data 1). For CRM sediments (BCR 667, NIST 8704 and NIST 1646a), the results showed mean recoveries of 86% with a mean precision of 4% RSD for all REEs and mean recoveries of 97% with mean precision of 11% RSD for all other trace metals (Supplementary Data 1).

Evaluation of Rare Earth Element Anomalies

The dissolved and particulate patterns are using the European Shale Composite (EUS) as a reference for normalization (Bau et al. 2018). Lanthanum, Ce and Gd anomalies (La*, Ce*, and Gd*) were calculated as follows (Elbaz-Poulichet et al. 2002; Kulaksız and Bau 2011b; Lerat-Hardy et al. 2019; Song et al. 2017), and there is a positive anomaly when the value of La*, Ce*, and Gd* is greater than 1.8:

$$[\text{La}_{\text{nat}}] = 10^{(3 \times \log(\text{Pr}_{\text{SN}}) - 2 \times \log(\text{Nd}_{\text{SN}}))} \times [\text{La}_{\text{EUS}}] \quad (1)$$

$$[\text{Ce}_{\text{nat}}] = 10^{(0.5 \times \log(\text{La}_{\text{SN}}) + 0.5 \times \log(\text{Pr}_{\text{SN}}))} \times [\text{Ce}_{\text{EUS}}] \quad (2)$$

$$[\text{Gd}_{\text{nat}}] = 10^{(0.2 \times \log(\text{Nd}_{\text{SN}}) + 0.8 \times \log(\text{Tb}_{\text{SN}}))} \times [\text{Gd}_{\text{EUS}}] \quad (3)$$

$$[\text{REE}_{\text{anthr}}] = [\text{REE}_{\text{measured}}] - [\text{REE}_{\text{nat}}] \quad (4)$$

$$[\text{REE}^*] = \frac{[\text{REE}_{\text{SN}}]}{[\text{REE}_{\text{SN}}^{\text{nat}}]} \quad (5)$$

where REE_{SN} is the concentration of a REE normalized by the concentration of the same REE of the EUS; [REE_{nat}] represents the natural concentration of the REE studied; [REE_{EUS}] is the REE concentration studied for EUS; [REE*] represents the anomaly value of the REE studied.

Table 1 Analytical quality monitoring using some certified reference materials for water (NCR SLRS-6) and sediments (BCR 667, NIST 8704, NIST 1646a)

	V	Cr	Co	Ni	Cu	Zn	As	Sr	Mo	Ag	Cd	Sn	Sb	Ba	Pb	Th	U	Al	Fe
NRC SLRS-6 (ng L ⁻¹)	Measured	0.359 ± 0.024	0.255 ± 0.022	0.053 ± 0.002	0.597 ± 0.051	22.3 ± 1.16	1.71 ± 0.406	0.573 ± 0.054	38.2 ± 1.83	0.184 ± 0.009	N.D.	0.007 ± 0.001	N.D.	0.32 ± 0.02	13.2 ± 0.527	0.157 ± 0.01	N.D.	0.061 ± 0.004	N.D.
	Certified	0.351 ± 0.006	0.252 ± 0.012	0.053 ± 0.012	0.616 ± 0.022	23.5 ± 1.8	1.76 ± 0.12	0.57 ± 0.08	40.66 ± 1.826	0.215 ± 0.018	N.D.	0.0063 ± 0.0014	N.D.	0.3372 ± 0.0058	14.28 ± 0.48	0.17 ± 0.026	N.D.	0.0698 ± 0.0034	N.D.
BCR 667 (mg kg ⁻¹)	Measured	N.D.	174 ± 14	22.1 ± 1.6	127 ± 12	61.6 ± 5.3	161 ± 24	17.8 ± 2.5	222 ± 11	N.D.	0.65 ± 0.056	N.D.	0.82 ± 0.063	N.D.	30.4 ± 1.16	9.1 ± 0.93	1.98 ± 0.122	N.D.	N.D.
	Certified	N.D.	178 ± 16	23 ± 1.3	128 ± 9	60 ± 9	175 ± 13	N.D.	N.D.	N.D.	N.D.	0.67 ± 0.05	0.96 ± 0.063	N.D.	N.D.	10 ± 0.5	2.26 ± 0.15	N.D.	N.D.
NIST 8704 (mg kg ⁻¹)	Measured	92.2 ± 5.4	112 ± 7.02	12.8 ± 0.75	41.5 ± 3.3	N.D.	366 ± 51	N.D.	N.D.	N.D.	3.20 ± 0.22	N.D.	2.68 ± 0.27	398 ± 28	141 ± 14	8.39 ± 1.3	2.76 ± 0.18	N.D.	N.D.
	Certified	94.6 ± 4	121.9 ± 3.8	13.57 ± 0.43	42.9 ± 3.7	N.D.	408 ± 15	N.D.	N.D.	N.D.	2.94 ± 0.29	N.D.	3.07 ± 0.32	413 ± 13	150 ± 17	9.07 ± 0.16	3.09 ± 0.13	N.D.	N.D.
NIST 1646a (mg kg ⁻¹)	Measured	41.5 ± 3.14	36.0 ± 2.74	N.D.	N.D.	10.2 ± 0.97	49.3 ± 4.5	6.46 ± 0.37	N.D.	N.D.	0.201 ± 0.17	N.D.	N.D.	N.D.	11.5 ± 1.01	N.D.	N.D.	N.D.	N.D.
	Certified	44.84 ± 0.76	40.9 ± 1.9	N.D.	N.D.	10 ± 0.34	48.9 ± 1.6	6.23 ± 0.21	N.D.	N.D.	0.148 ± 0.007	N.D.	N.D.	N.D.	11.7 ± 1.2	N.D.	N.D.	N.D.	N.D.
	Values	La	Ce	Pr	Nd	Sm	Eu	Gd	Tb	Dy	Ho	Er	Tm	Yb	Lu				
NRC SLRS-6 (ng L ⁻¹)	Measured	235 ± 19.0	281 ± 22.5	58.6 ± 4.96	221 ± 12.7	38.4 ± 2.31	6.23 ± 0.71	28.1 ± 1.72	3.46 ± 0.25	19.5 ± 1.39	3.93 ± 0.39	11 ± 0.76	1.56 ± 0.17	10.2 ± 1.04	1.59 ± 0.28				
	Certified	248 ± 12.1	292 ± 15.1	59.1 ± 1.9	227 ± 9.4	39.5 ± 1.7	7.26 ± 0.35	31.6 ± 2.5	4.07 ± 0.27	21.9 ± 1.1	4.3 ± 0.3	12.4 ± 0.7	1.79 ± 0.18	11.2 ± 0.7	1.91 ± 0.23				
BCR 667 (mg kg ⁻¹)	Measured	25.1 ± 1.62	50.6 ± 3.47	6.08 ± 0.44	22.6 ± 0.55	4.64 ± 0.13	0.902 ± 0.03	3.79 ± 0.14	0.543 ± 0.02	3.35 ± 0.07	0.662 ± 0.02	1.84 ± 0.04	0.265 ± 0.01	1.68 ± 0.05	0.245 ± 0.01				
	Certified	27.8 ± 1.0	56.7 ± 2.5	6.1 ± 0.50	25 ± 1.4	4.66 ± 0.20	1 ± 0.05	4.41 ± 0.12	0.682 ± 0.017	4.01 ± 0.14	0.8 ± 0.06	2.35 ± 0.15	0.326 ± 0.025	2.2 ± 0.09	0.325 ± 0.02				

N.D., undefined elements

Estimation of Trace Metal and REE Fluxes

Metal fluxes at the NBH collector site were calculated from the following equations:

$$X_{\text{dissolved}} \text{ flux} = \sum (V_i \times [X_{\text{dissolved}}]_i) \times T_i \quad (6)$$

where V_i is the water volume at a sampling time; $[X_{\text{dissolved}}]_i$ the dissolved concentration of the element expressed in $\mu\text{g L}^{-1}$; T_i is the sampling duration at a sampling time.

$$X_{\text{particulate}} \text{ flux} = \sum ([\text{SPM}]_i \times V_i \times [X_{\text{particulate}}]_i) \times T_i \quad (7)$$

where $[\text{SPM}]_i$ is the SPM concentration at a sampling time; V_i the corresponding water volume at a sampling time; $[X_{\text{particulate}}]_i$ the concentration of the particulate element expressed in mg kg^{-1} ; T_i is the sampling duration at a sampling time.

Metal fluxes at the JR site were calculated from the following equations:

$$X_{\text{dissolved}} \text{ flux} = \sum (Q_h \times [X_{\text{dissolved}}]_h) \quad (8)$$

where Q_h is the hourly discharges at a sampling time and $[X_{\text{dissolved}}]_h$ the mean hourly concentrations of the element.

$$X_{\text{particulate}} \text{ flux} = \sum ([\text{SPM}]_h \times Q_h \times [X_{\text{particulate}}]_h) \quad (9)$$

where $[\text{SPM}]_h$ is the mean hourly SPM concentration; Q_h the hourly discharge; and $[X_{\text{particulate}}]_h$ the mean hourly particulate concentration of the element expressed in mg kg^{-1} .

Data Treatment

Given the large number of elements, a statistical approach using hierarchical cluster analysis was performed to identify and quantify the complex relationships between trace metals, and analyze their evolution during the hydrological event. A heatmap was performed by using hierarchical cluster analysis from the standardized variables, with Euclidean distances and Ward's linkage criteria. This method is performed for individuals (sampling periods) and variables (physical and chemical parameters, trace metal and REE concentrations in dissolved and particulate expressed in $\mu\text{g L}^{-1}$), allowing to obtain two dendrograms. From these dendrograms, a heatmap can be drawn to characterize clusters: red tones identify clusters with high values for the corresponding variables, whereas low values tend to blue tones.

Results

Water Discharge, SPM Concentrations, Physical and Chemical Parameters

The base level of discharge at the NBH collector site in dry weather is $0.015 \text{ m}^3 \text{ s}^{-1}$ (data not shown). During the rainy event, instantaneous discharge (Q_i) showed high temporal variability increasing from $1.60 \text{ m}^3 \text{ s}^{-1}$ at 7:20 PM to a peak of $4.40 \text{ m}^3 \text{ s}^{-1}$ at 7:42 PM, followed by a decrease to $0.90 \text{ m}^3 \text{ s}^{-1}$ at 11:30 PM (Fig. 2). The hourly Jalle River discharges at the JR site generally increased between 6:30 PM and 2:30 AM with a temporary maximum of $4.05 \text{ m}^3 \text{ s}^{-1}$ at 8:30 PM (Fig. 2) and slowly decreased between 2:30 AM and 12:30 PM to its base level of $0.26 \text{ m}^3 \text{ s}^{-1}$.

Compared with the low SPM concentration usually measured during low water conditions ($\sim 4.0 \text{ mg L}^{-1}$; data not shown), instantaneous SPM concentrations at the NBH collector site were extremely high (700 mg L^{-1}) at 7:20 PM, i.e., at the beginning of the first flush and then gradually decreased by a factor 50 until the end of the event (14.0 mg L^{-1} at 11:30 PM—Fig. 2). The SPM concentration at the JR site remained relatively low ($\sim 2.50 \text{ mg L}^{-1}$) throughout the event, except for a sharp SPM peak at 8:30 PM (630 mg L^{-1}) followed by a rapid decrease to baseline values (Fig. 2).

At the NBH collector site, nitrogen concentrations decreased from the beginning of the event to the end (from 6.40 to $< 1.00 \text{ mg L}^{-1}$ —Supplementary Data 2). Similarly, biological oxygen demand (X5-BOD) and chemical oxygen demand (COD) levels decreased by one order of magnitude throughout the rain event (X5-BOD: from 42.0 to 4.00 mg L^{-1} , COD: from 265 to 27.6 mg L^{-1} —Supplementary Data 2). Finally, dissolved organic carbon (DOC) concentrations, at the NBH collector site, decreased during the event (23.5 – 7.00 mg L^{-1}), except for one sample (8:30 PM), where DOC temporarily reached a concentration similar to those at the beginning of the observation period (Supplementary Data 2).

At the JR site, temperature (Temp) slightly decreased stepwise: from $21.6 \pm 0.3 \text{ }^\circ\text{C}$ before the rainy event to $20.4 \pm 0.1 \text{ }^\circ\text{C}$ between 8:30 PM and 4:30 AM and to $19.5 \pm 0.1 \text{ }^\circ\text{C}$ between 8:30 and 11:30 AM (Supplementary Data 2). Dissolved oxygen concentrations (O_2) showed diel variations with highest values during daytime, mainly increasing during the afternoon (from 6.00 mg L^{-1} at 1:30 PM to 7.90 mg L^{-1} at 6:30 PM—Supplementary Data 2), and lowest values (3.60 mg L^{-1}) during the night at 4:30–5:30 AM (Supplementary Data 2). The pH values increased from 7.58 at 4:30 PM to 7.81 at 8:30 PM, then decreased to $\sim 7.42 \pm 0.01$ from 4:30 AM until the end

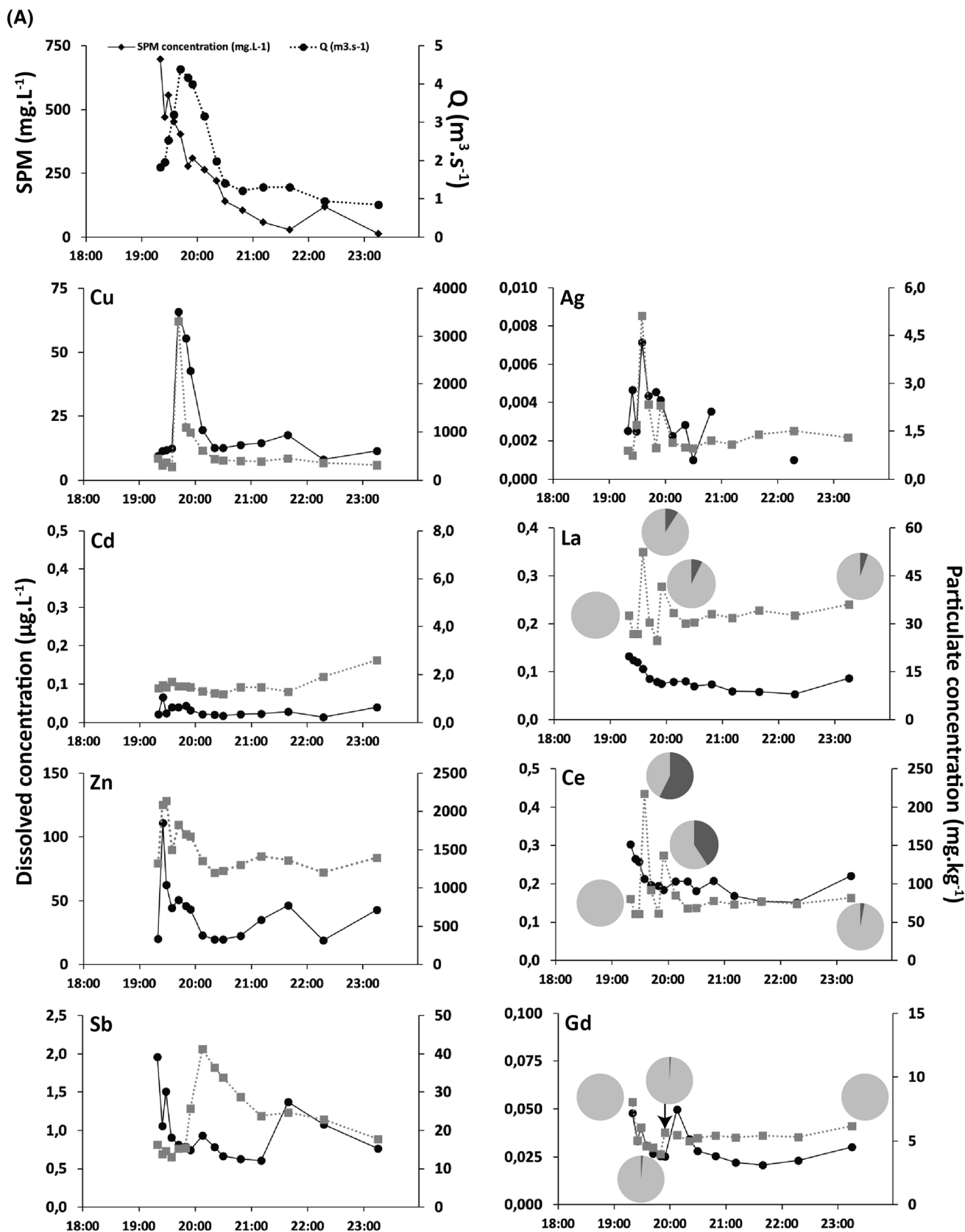


Fig. 2 Temporal evolution of water discharges (Q) and SPM concentrations in **a** the NBH collector and **b** the Jalle River during the rainstorm. Chemographs of Cu, Cd, Zn, Sb, Ag, La, Ce, and Gd for the dissolved phase (black line and black circle on y-axis) and particulate phase (dotted gray and gray square on secondary y'-axis) for

both sites. REE partitioning for La, Ce, and Gd indicated by pie charts with the portion of Aqua Regia extraction represented by light gray. The dark gray portions represent the residual fraction defined by the difference between HCl/HNO₃/HF and Aqua Regia fraction

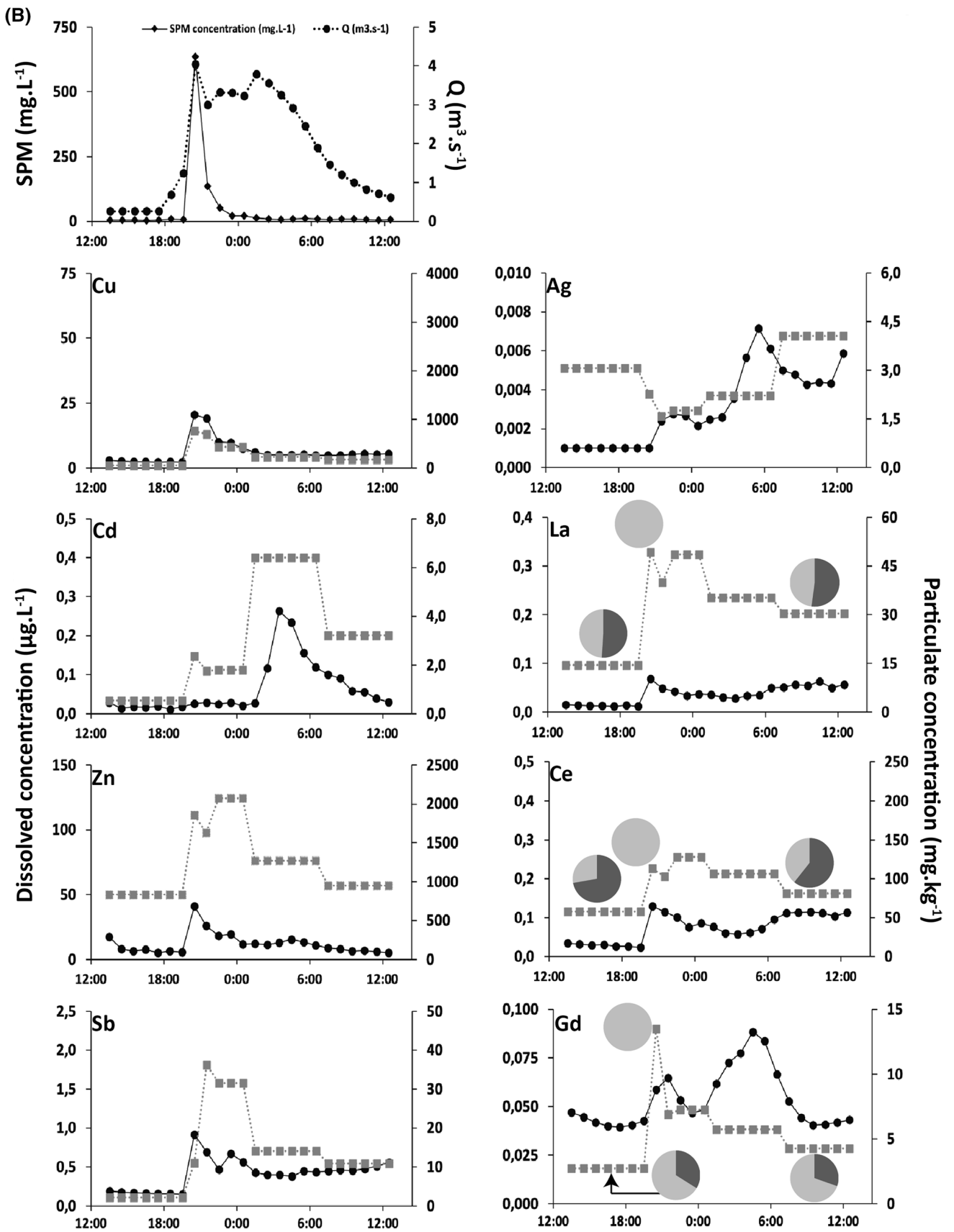


Fig. 2 (continued)

of the monitoring (Supplementary Data 2). Conductivity (Cond) showed distinct temporal evolutions with a baseline of $\sim 532 \pm 3.00 \mu\text{S cm}^{-1}$ before the rainy period, a decline to $245 \pm 17.0 \mu\text{S cm}^{-1}$ from 8:30 PM to 11:30 PM, an increase to $410 \pm 17.0 \mu\text{S cm}^{-1}$ at 3:30–4:30 AM and then remained stable $\sim 290 \pm 1.00 \mu\text{S cm}^{-1}$ (Supplementary Data 2).

Metal Concentrations at the Northern Bordeaux Highway (NBH) Collector Site

The summary of the statistical parameters (minimum, maximum, median, and mean values) of dissolved and particulate metal concentrations measured at the NBH collector site are shown in Table 2. Dissolved and particulate concentration amplitudes (defined as the ratio of the maximum over the minimum values) covered more than one order of magnitude with different patterns depending on the element. The obtained concentration ratios ranged from 1.8 (Th) to 19 (Co) in the dissolved phase and from 1.3 (Ni) to 12 (Cu) in the particulate phase. When regarding the particulate loads, i.e., the particulate fraction including SPM concentrations and expressed in $\mu\text{g L}^{-1}$, the ratios varied from 27 (Cd) to 305 (Cu) (Table 2).

In the dissolved phase, classical trace metals showed one (e.g., Cu_d) or more (e.g., Sb_d) peaks at different sampling times (Fig. 2). Dissolved REE concentrations, except Gd_d , continuously decreased during the rainy event (Fig. 2). Particulate V and Th_p were negatively correlated with SPM ($R^2 = -0.87$ and -0.90) and showed low concentrations during the first minutes of the rain event. For these elements, concentrations increased during the event. Other elements showed one (e.g., Cu_p) or more peaks (e.g., Ag_p) at different sampling times, largely independent from the SPM concentrations (Fig. 2). In contrast, particulate REEs except La_p and Ce_p continuously decreased throughout the sampling period as observed for SPM concentrations (Fig. 2).

At the NBH collector site, the dissolved patterns showed a slight enrichment toward Heavy Rare Earth Elements (HREEs) (Fig. 3). Conversely, particulate patterns showed a slight depletion toward HREEs (Fig. 3). With maximum values of 1.6, 1.8, and 2.2 for La_d^* , Ce_d^* , and Gd_d^* and 2.2, 2.6, and 1.2 for La_p^* , Ce_p^* , and Gd_p^* at the NBH collector site, there are clear anomalies for La_p and Ce_p , whereas Gd_d only showed an anomaly in one sample (at 8:08 PM, sample 8).

For each sample, particulate metal concentrations were compared to total (particulate + dissolved) metal concentrations establishing statistical (Boxplot) distributions (Fig. 4). At the NBH collector site, the particulate phase was largely dominant. In fact, median values ranged from 84.3 to 99.7% for all classic trace metals and REEs, except for Mo (60.8%) and Sr (46.0%) (Fig. 4). However, partitioning varied throughout the

event, with the highest particulate proportion occurring during the first flush.

Metal Concentrations in the Jalle River (JR Site)

The summary of the statistical parameters (minimum, maximum, median, and mean values) of dissolved and particulate metal concentrations measured at the JR site are presented in Table 2. At the Jalle River site, temporal variability (expressed as the ratio of the maximum over the minimum values) strongly differed from one element to another. The obtained concentration ratios ranged from 1.4 (As) to 23 (Cd) in the dissolved phase and from 1.3 (Sr) to 17 (Sb) in the particulate phase expressed in mg kg^{-1} . The particulate loads expressed in $\mu\text{g L}^{-1}$ showed ratios from 159 (Ba) to ~ 4000 (Cu) (Table 2).

Dissolved Cu, Zn_d, Sb_d, La_d, and Ce_d showed a peak at 8:30 PM (Fig. 2). Conversely, Cd_d, Ag_d, and Gd_d showed their highest levels later in the night (Fig. 2). For most elements, the highest particulate concentrations occurred together with the maximum SPM concentration (e.g., Cu_p, Zn_p, Sb_p, La_p, Ce_p, and Gd_p; Fig. 2). In contrast, Ag_p concentrations showed the lowest values with the maximum SPM concentration (Fig. 2). Similar to Cd_d, Cd_p reached its maximum later in the night (Fig. 2).

At the JR site, the dissolved REE patterns showed a slight enrichment toward HREEs (Fig. 3). This trend is more pronounced for samples before 9:30 PM (before and during the rainy event). Particulate patterns showed a slight depletion towards HREEs (Fig. 3). The JR site was characterized by high Gd_d* (maximum value = 10) and Ce_p* (maximum value = 2.0). Similarly, the JR site presented moderate La_p* (maximum value = 1.8).

As for the NBH collector site, particulate concentrations were compared to total (particulate + dissolved) concentrations (Fig. 4). At the JR site, statistical distribution displayed full range of variations with variable particulate contribution depending on the sample and the element. Median values were > 50% for Ag, Sn, Pb, Th, Cr, Co, Zn, and all REEs, except Gd (Fig. 4). In contrast, Gd, Cd, V, Cu, Ni, Ba, Sb, U, As, Mo, and Sr had median values < 40% (Fig. 4). As a result, the dissolved phase was dominant throughout nearly the whole rain event, except at the time of the SPM peak (8:30 PM and 9:30 PM; Fig. 2), when the particulate phase was dominant for all classic trace metals (except Sr) and REEs.

Discussion

Impact of Rainy Events on SPM and Trace Metals Transport at the NBH Collector Site

The hierarchical cluster analysis was interpreted from the variables (e.g., classical trace metal and REE

Table 2 Summary of the statistical parameters (minimum, maximum, median, and mean values) of the metal concentrations (dissolved and particulate phases) measured at the NBH collector and the JR sites

NBH collector																		
Dissolved ($\mu\text{g L}^{-1}$)						Particulate (mg kg^{-1})						Particulate ($\mu\text{g L}^{-1}$)						
Min	Max	Median	Mean	Max/Min		Min	Max	Median	Mean	Max/Min		Min	Max	Median	Mean	Max/Min		
La	0.05	0.13	0.079	0.086	Th	1.8	24.8	52.6	32.6	33.2	Ni	1.3	0.51	23.8	6.91	9.11	Cd	27
Ce	0.15	0.3	0.206	0.208	Al	1.9	60.8	217	76.8	87.6	Pb	1.4	1.15	98.5	17.0	25.7	U	28
Pr	0.02	0.05	0.028	0.029	Ce	2.0	5.8	9.59	7.85	7.74	Mo	1.5	0.13	6.68	1.61	2.11	Co	28
Nd	0.09	0.22	0.138	0.14	Sm	2.0	24.2	42	32.1	31.9	Sn	1.5	0.51	29.3	6.72	8.89	Th	32
Sm	0.03	0.06	0.048	0.047	As	2.0	5.01	9.27	6.71	6.67	Sr	1.5	0.11	6.46	1.39	1.86	As	32
Gd	0.02	0.05	0.028	0.031	Pr	2.3	3.98	8.06	5.29	5.41	V	1.5	0.09	5.61	1.11	1.54	Al	35
Tb	0	0.01	0.003	0.004	V	2.4	0.53	0.995	0.699	0.700	Fe	1.6	0.01	0.693	0.150	0.197	V	37
Dy	0.02	0.04	0.021	0.023	Gd	2.4	3.26	6.19	4.25	4.28	Ba	1.6	0.07	4.32	0.906	1.22	Fe	38
Ho	0	0.01	0.004	0.005	Dy	2.4	0.663	1.25	0.843	0.853	Cr	1.6	0.01	0.874	0.184	0.243	Cr	41
Er	0.01	0.03	0.012	0.014	Tb	2.4	1.82	3.35	2.26	2.31	Yb	1.6	0.04	2.34	0.506	0.658	Ni	45
Tm	0	0	0.002	0.002	La	2.5	0.243	0.45	0.308	0.316	Pr	1.7	0.01	0.314	0.067	0.089	Sb	45
Yb	0.01	0.03	0.012	0.014	Nd	2.5	1.71	2.74	2.01	2.02	Lu	1.7	0.03	1.91	0.478	0.572	La	47
Lu	0	0.01	0.002	0.002	Cr	2.5	0.219	0.378	0.270	0.277	Nd	1.7	0	0.264	0.061	0.078	Mo	50
V	1.11	2.65	1.77	1.84	Ba	2.6	93.5	145	118	118	Al	1.8	1.9	70.1	29.3	29.7	Pr	52
Cr	0.33	0.83	0.591	0.601	Ho	2.6	72.7	115	91.3	91.4	Zn	1.8	1.25	51.2	23.0	23.7	Sn	53
Co	0.09	1.65	0.309	0.463	Ni	2.6	18.8	53.7	28.3	31.3	Th	1.8	0.67	18.8	7.87	7.45	Pb	55
Ni	0.75	1.93	0.994	1.07	Er	2.6	30.8	38.7	35.4	34.8	Er	1.8	0.5	22.5	9.32	9.28	Nd	57
Cu	8.06	65.7	12.6	21.2	Tm	2.7	283	3306	404	675	Sm	1.8	4.37	1332	128	211	Sm	58
Zn	19.1	111	42.8	40.5	Yb	3.2	1201	2138	1395	1514	Tm	1.9	19.6	1189	357	448	Lu	59
As	0.59	1.21	0.695	0.734	Sb	3.2	13.7	29.9	17.5	19.00	Tb	1.9	0.42	13.6	4.36	4.74	Yb	60
Sr	20.3	74.4	24.8	30.9	Lu	3.3	65.6	101	80.7	81.5	Ho	1.9	0.93	56.1	21.1	23.2	Sr	60
Mo	0.62	2.56	0.706	0.955	Sr	3.7	3.97	5.83	4.70	4.87	Dy	1.9	0.07	3.24	1.18	1.31	Zn	61
Ag	0	0.01	0.003	0.003	Pb	3.8	0.741	5.12	1.20	1.58	Gd	2	0.02	2.32	0.269	0.483	Tm	61
Cd	0.01	0.07	0.024	0.03	Sn	3.9	1.19	2.61	1.48	1.55	La	2.1	0.04	0.994	0.347	0.41	Ba	62
Sn	0.05	0.18	0.078	0.093	Mo	4.1	30	44.3	34.9	35.4	As	2.2	0.45	23.6	8.71	9.57	Er	63
Sb	0.61	1.96	0.817	0.975	Fe	4.1	13.1	41.3	22.8	22.9	Cd	2.2	0.25	11.4	5.93	5.48	Ho	63
Ba	8.86	22.7	11.5	13.2	Cd	4.6	294	460	367	365	U	2.2	4.16	256	97.5	106	Tb	63
Pb	0.27	1.02	0.530	0.582	U	5.1	100	142	114	113	Co	2.9	1.5	82.6	28.2	30.9	Dy	63
Th	0.01	0.02	0.015	0.015	Zn	5.8	4.29	7.76	6.05	5.9	Sb	3.2	0.1	3.23	1.41	1.42	Gd	65
U	0.04	0.22	0.072	0.09	Ag	7.1	1.5	3.36	1.82	2.04	Ce	3.6	0.05	1.33	0.44	0.488	Ce	86
Al	26.7	50.4	37.4	36.8	Cu	8.1	41,481	72,979	57,071	54,821	Ag	6.9	885	31,073	13,395	13,255	Ag	127
Fe	51.1	210	83.8	92.2	Co	19	33,181	51,940	40,731	41,488	Cu	12	729	27,924	9768	10,514	Cu	305

Table 2 (continued)

JR Site	Particulate (mg kg ⁻¹)													
	Min	Max	Median	Mean	As	Max/Min	La	Min	Max	Median	Mean	Sr	Max/Min	Max/Min
La	0.012	0.069	0.036	0.036	As	1.4	La	14.6	49.3	37.6	36.4	Sr	1.3	1.3
Ce	0.024	0.130	0.076	0.075	Cr	1.5	Ce	58.1	128	104	98.2	Ba	1.7	1.7
Pr	0.005	0.024	0.011	0.012	V	1.6	Pr	3.61	14.5	8.97	9.10	Ce	2.2	2.2
Nd	0.027	0.123	0.055	0.057	Gd	2.2	Nd	14.8	65.4	35.3	36.8	Ni	2.4	2.4
Sm	0.014	0.040	0.021	0.022	Sr	2.4	Sm	3.16	15.0	7.49	7.95	U	2.5	2.5
Gd	0.039	0.088	0.047	0.053	Ba	2.6	Gd	2.75	13.5	6.32	6.74	Zn	2.5	2.5
Tb	0.001	0.005	0.002	0.002	Mo	2.7	Tb	0.372	1.64	0.779	0.84	Ag	2.6	2.6
Dy	0.009	0.035	0.014	0.015	Sm	2.9	Dy	2.15	10.2	4.80	5.16	Th	2.8	2.8
Ho	0.002	0.009	0.003	0.003	Ni	3.1	Ho	0.439	2.08	0.911	1.02	Sn	3.0	3.0
Er	0.006	0.031	0.009	0.011	Al	3.1	Er	1.20	5.73	2.50	2.79	Cr	3.1	3.1
Tm	0.001	0.005	0.001	0.002	Tb	3.6	Tm	0.156	0.782	0.347	0.384	La	3.4	3.4
Yb	0.007	0.042	0.010	0.014	Dy	3.7	Yb	1.09	4.89	2.05	2.35	Pr	4.0	4.0
Lu	0.001	0.007	0.002	0.002	Ho	4.0	Lu	0.137	0.718	0.309	0.342	As	4.1	4.1
V	1.08	1.74	1.57	1.52	U	4.1	V	29.5	151	104	102	Pb	4.3	4.3
Cr	0.397	0.596	0.488	0.480	Fe	4.4	Cr	45.8	142	94.1	93.9	Tb	4.4	4.4
Co	0.109	0.684	0.166	0.196	Nd	4.6	Co	10.3	65.2	33.2	35.6	Nd	4.4	4.4
Ni	0.995	3.05	1.64	1.74	Pb	4.7	Ni	24.8	58.9	44.8	44.5	Yb	4.5	4.5
Cu	2.23	20.6	5.07	6.08	Er	4.8	Cu	47.5	759	332	388	Ho	4.7	4.7
Zn	5.31	41.3	9.95	12.2	Tm	4.9	Zn	836	2075	1452	1436	Dy	4.7	4.7
As	0.731	1.06	0.954	0.922	Th	5.1	As	11.2	45.6	24.9	26.2	Sm	4.8	4.8
Sr	62.8	152	87.5	102	Pr	5.2	Sr	91.5	122	104	104	Er	4.8	4.8
Mo	0.447	1.23	0.628	0.626	Ce	5.4	Mo	1.24	6.76	3.92	3.98	Gd	4.9	4.9
Ag	0.001	0.007	0.003	0.003	La	5.6	Ag	1.59	4.06	2.25	2.50	Tm	5.0	5.0
Cd	0.011	0.263	0.029	0.064	Yb	5.8	Cd	0.534	6.42	2.08	2.68	V	5.1	5.1
Sn	0.033	0.247	0.090	0.108	Lu	6.0	Sn	22.9	69.1	41.1	42.4	Lu	5.2	5.2
Sb	0.150	0.917	0.439	0.410	Sb	6.1	Sb	2.16	36.3	12.5	17.6	Mo	5.5	5.5
Ba	12.3	32.0	16.0	17.0	Co	6.3	Ba	391	650	418	466	Co	6.4	6.4
Pb	0.070	0.324	0.236	0.208	Ag	7.1	Pb	36.1	155	116	111	Cd	12	12
Th	0.007	0.035	0.014	0.016	Sn	7.4	Th	4.26	11.8	8.16	8.12	Cu	16	16
U	0.076	0.313	0.117	0.155	Zn	7.8	U	1.13	2.8	2.61	2.28	Sb	17	17
Al	13.6	42.0	23.1	22.3	Cu	9.2	Al	N.D	N.D	N.D	N.D	Al	N.D	N.D
Fe	28.0	123	59.3	69.6	Cd	23.4	Fe	N.D	N.D	N.D	N.D	Fe	N.D	N.D

For both sampling sites, and for both phases, the max/min concentration ratio was determined, and the elements were then ordered in increasing order

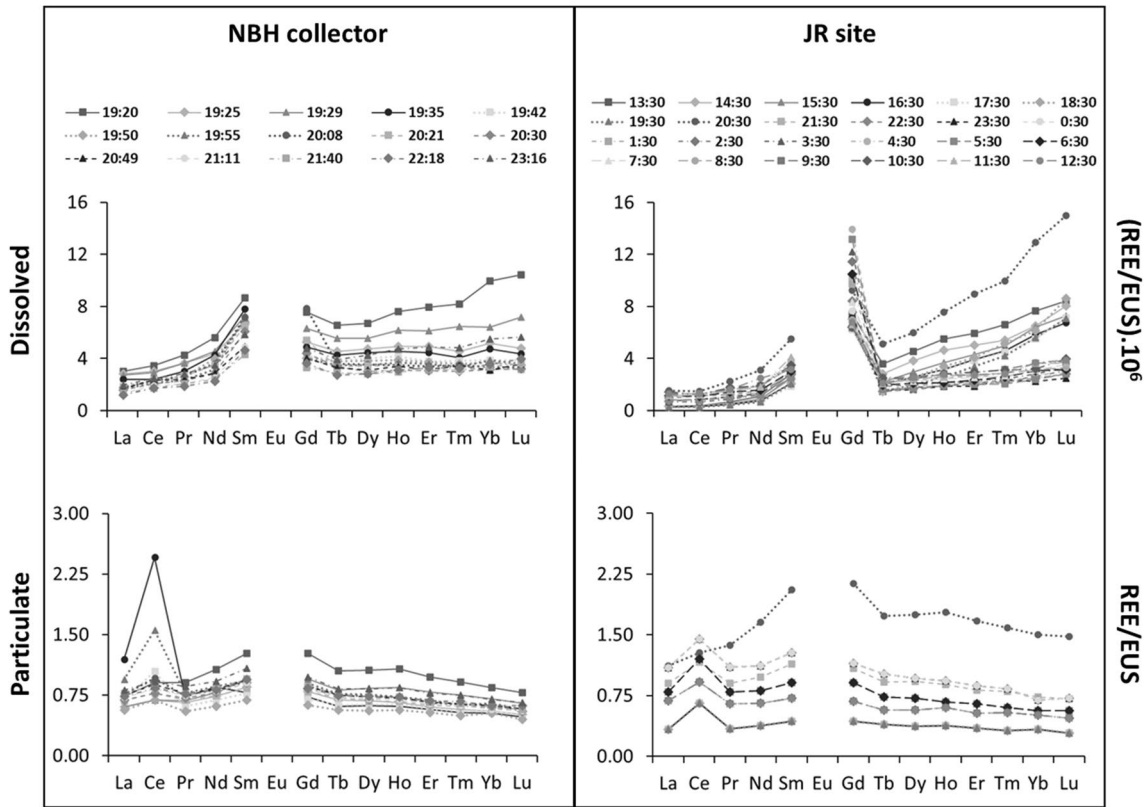


Fig. 3 EUS-normalized concentration patterns for dissolved and particulate phases at the NBH collector and the JR sites

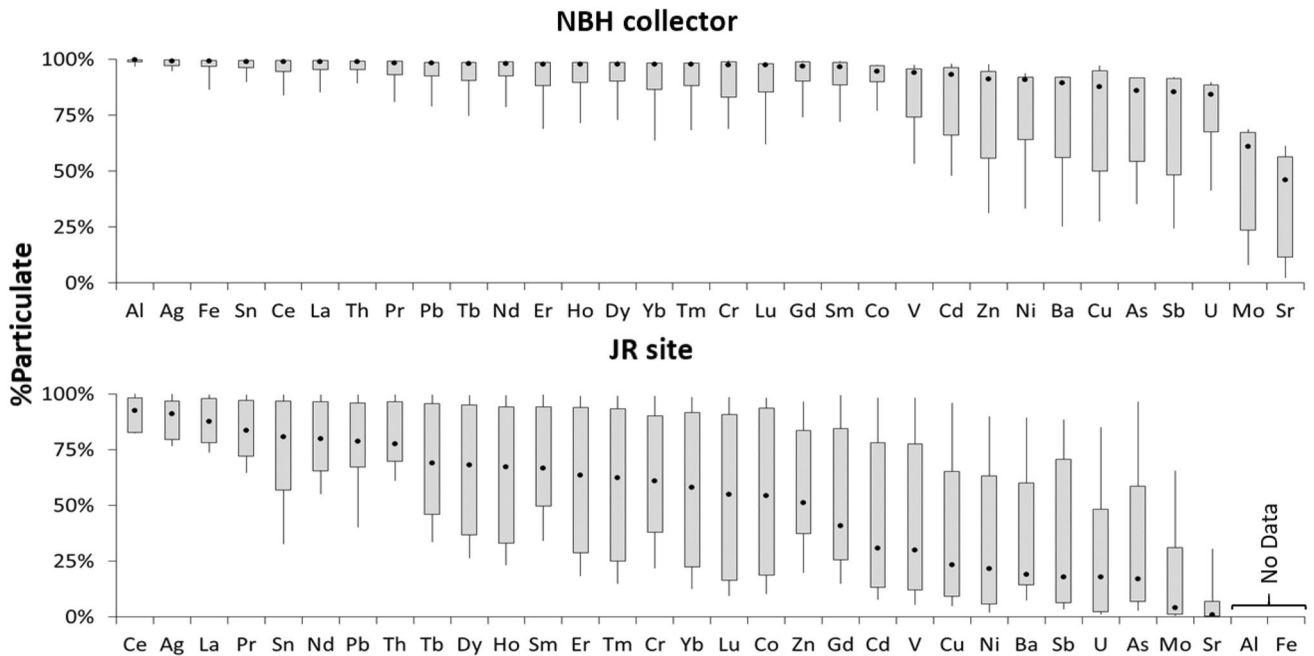


Fig. 4 Distribution of the relative particulate metal contributions for the NBH collector and the JR sites

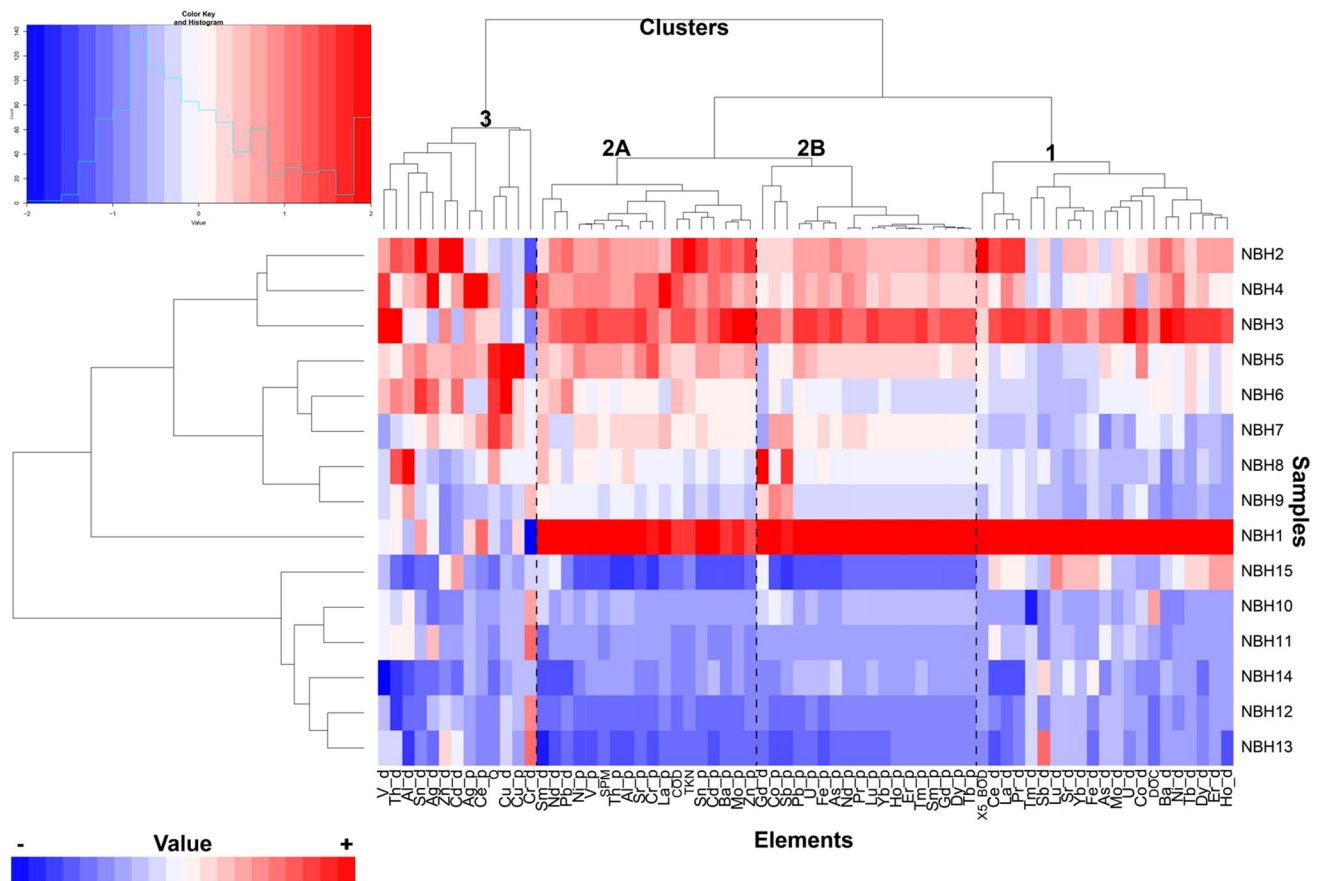


Fig. 5 Statistical approach (Heatmap) for samples collected at the NBH collector site. Red tones identify clusters with high values for the corresponding variables, whereas low values tend to blue tones. The dashed lines are provided to separate the different clusters

concentrations) to identify the existence/dominance of common metal sources and/or transport during the rainy event. The hierarchical cluster analysis at the NBH collector site suggests three distinct clusters.

The cluster 1 regroups X5-BOD, DOC, Ce_d , La_d , Pr_d , As_d , Mo_d , U_d , Co_d , Ni_d , Ba_d , Yb_d , Sr_d , Lu_d , Dy_d , Tb_d , Tm_d , Er_d , Ho_d , Sb_d , and Fe_d (Fig. 5). Elements belonging to this cluster show the highest concentrations at the beginning of the monitoring and a general decrease during the rainy event (Ce_d , La_d , Pr_d , As_d , Mo_d , U_d , Co_d , Ni_d , Ba_d , Yb_d , Sr_d , Lu_d , Dy_d , Tb_d , Tm_d , Er_d , Ho_d , and Sb_d ; Fig. 2), with possible moderate peaks at different sampling times depending on the element (i.e. La_d , Ce_d , and Sr_d ; Fig. 2). The maximum values observed at the beginning of the rainy event were similar to recent mean values (unpublished data) observed in dry conditions. Because the NBH collector site does not only receive rainwater but has a low water support related to groundwater (mainly from calcareous aquifers), the observed decrease during the event suggests an effect of dilution of groundwater by rainwater, less concentrated in dissolved metals/REEs.

The second cluster (Cluster 2) can be subdivided into two subclusters (Fig. 5):

- Subcluster 2A represented by COD, TKN, SPM, Pb_d , Nd_d , Sm_d , Cd_p , Sn_p , Mo_p , Ba_p , Zn_p , Cr_p , V_p , Th_p , Sr_p , Ni_p , Al_p , and La_p ;
- Subcluster 2B represented by DOC, Tb_p , Dy_p , Gd_p , Sm_p , Ho_p , Tm_p , Er_p , Yb_p , Lu_p , Nd_p , Pr_p , U_p , Pb_p , As_p , Co_p , Sb_p , Fe_p , and Gd_d .

For the parameters grouped in Cluster 2, the concentrations are increasing to reach a peak at the beginning of the event and then decrease. Both subclusters of the Cluster 2 showed distinct behaviors with the highest concentrations with the SPM peak suggesting additional sources and/or sorption processes. The negative correlation between V_p and Th_p concentrations and SPM concentrations during the first flush suggests that the first flush is associated with coarse sediment transport leading to low concentrations of geogenic elements as previously shown in other systems (Furumai et al. 2002). Indeed, previous studies have shown that V and Th are clearly influenced by grain size at the regional

scale (Coynel et al. 2007, 2016). A chemical property of the lanthanides may explain the decrease of particulate REE concentrations as their atomic numbers increase. The ionic radius of REEs decreases from Light REEs (LREEs) to Heavy REEs (HREEs), resulting in an increase in the solubility constant from LREEs to HREEs (Sholkovitz 1992). As a result, LREEs are preferentially adsorbed to the surface of particles, whereas HREEs are preferentially present in the dissolved phase (Sholkovitz 1995).

The third cluster (Cluster 3) reflects the differences in temporal variability of Sn_d , Ag_d , Cd_d , Zn_d , V_d , Th_d , Cr_d , Cu_d , and Al_d compared with other dissolved elements (Fig. 5). Also, this cluster regroups Ce_p , Ag_p , and Cu_p . Even if there is no obvious common trend for these elements, their highest concentrations did not occur during the first sampling but when water discharges (Q) were high, as illustrated previously by Cu_d and Cu_p (Fig. 2).

Because the drainage area of NBH collector site is large, the different peaks of dissolved and particulate metals could indicate the rinsing of several areas (from proximal to most distal) with different characteristics. Indeed, the metals and their concentrations in road dust are highly dependent on the road surface and road traffic (vehicle speed, traffic intensity, proximity to acceleration, braking or congestion zones; Padoan et al. 2018). With a high temporal follow-up, successive emissions of road dust can be observed.

At the NBH collector site, the percentage of REEs extracted from Aqua Regia relatively to $\text{HCl}/\text{HNO}_3/\text{HF}$ concentrations differ from an element to another. The Aqua Regia fraction was $\sim 100\%$ for LREE and decreased with HREEs from 100% (Tb) to 82% (Lu). It is interesting to note that samples 4 and 7 for Ce_p show a gap between the two attacks in favor of the $\text{HCl}/\text{HNO}_3/\text{HF}$ digestion (Fig. 2). This difference can be explained by two distinct hypotheses: (i) the Aqua Regia digestion is insufficient to extract the high quantity of Ce; and (ii) the second hypothesis is that Ce in the catalytic converters is present in the form of nanoparticles (CeO_2 —Montini et al. 2016) fixed on a mineral structure (cordierite body and washcoat). Due to mechanical stress during operation, Ce is emitted together with washcoat and/or cordierite debris. As a result, the presence of hydrofluoric acid in the triacid attack could be more effective in extracting this form of Ce.

Impact of Rainy Events on SPM and Trace Metals Transport in Jalle River

Unlike the NBH collector site, the hierarchical cluster analysis for the JR site was interpreted from the individuals (samples) to highlight the temporal variability of the flood event in the Jalle River (Fig. 6). The hierarchical cluster analysis at the JR site shows 4 distinct clusters, each reflecting a different period during the flood event.

Period 1: Basic Discharge Signature in Low Water Condition

The first period covers the samples 1–7 (1:30 PM–7:30 PM), when Co_d , Ba_d , Lu_d , Er_d , Ni_d , U_d , Sr_d , and, to a lesser extent, Tb_d displayed high concentrations at the beginning and a decrease during the flood event (Fig. 6). The samples from the first period show the geochemical signature of the Jalle River in low water conditions prior to the flood event. This is supported by the high Sr_d concentrations, which show a hydrological support of the calcareous aquifers in the downstream watershed (Arrouays et al. 2015).

Period 2: Signals from Trace Metals Associated with Motor Vehicle Traffic

The second period represent one isolated sample (sample 8–8:30 PM) showing the highest dissolved classical trace metal and REE concentrations, especially for Zn_d , Cu_d , Ce_d , or La_d (Fig. 6) concomitant with the peak of water discharge and SPM concentrations (except for Cd_d , Sn_d , Th_d , Ag_d , and Al_d). These high values coincided with the maximum NBH collector inputs at the JR site (8:30 PM). In fact, the Jalle River is a slightly erosive system with low SPM concentrations, as observed for the SPM concentrations before/after the 8:30 PM peak. Therefore, it can be assumed that particulate metals associated with the SPM peak are mainly derived from road dust runoff (composed of a mixture of natural and anthropogenic sources) from NBH collector site. Accordingly, the NBH collector inputs have a real impact on the Jalle River metal transport for Cu, Zn, Sb, Pb, Co, Cd, La, and Ce. These metals, identified as markers of the automotive activity, displayed concentrations similar to those reported for urban highways (Huber et al. 2016). Copper and Zn are present in several structural elements of motor vehicles, such as brake pads, tires, batteries, oils, and engine greases (Ball et al. 1998; Davis et al. 2001; Martínez and Poleto 2014; McKenzie et al. 2009; Sternbeck et al. 2002; von Uexküll et al. 2005). Zn also is used for the manufacture of safety fences (Dierkes and Geiger 1998) and asphalt (Martínez and Poleto 2014). Antimony is regularly studied to describe the highway source because of its frequent use for brake pads, lubricants, tires, and in engine alloys (Fujiwara et al. 2011; von Uexküll et al. 2005). Lead is used in various automotive parts, in paints, and has served for decades as an additive in gasoline for its anti-knock power, although Pb concentrations have continuously decreased during the past two decades due to its substitution in different emitting sources (Ball et al. 1998; Berbee et al. 1999; Legret and Pagotto, 1999; Kayhanian, 2012; Mangani et al. 2005). Cobalt is poorly documented in environmental studies. However, in the present study, the mean total Co (dissolved + particulate) concentration at

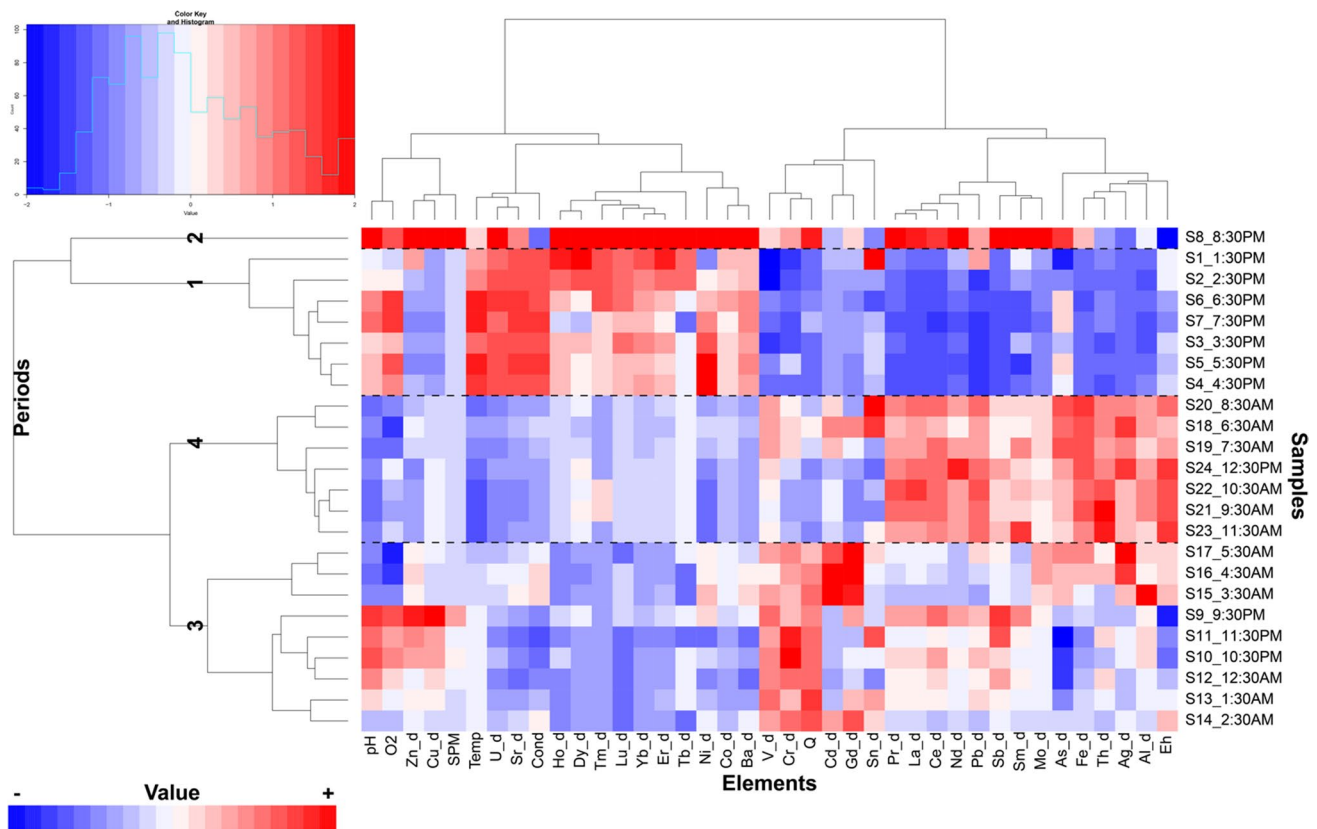


Fig. 6 Statistical approach (Heatmap) for samples (marked by an *S* on the figure) collected in the Jalle River (JR site). Red tones identify clusters with high values for the corresponding variables, whereas low values tend to blue tones. The hierarchical cluster analysis shows

four distinct clusters, each reflecting a different period during the flood event. Dashed lines are provided to separate the different periods

the NBH collector site was $7.90 \mu\text{g L}^{-1}$, which is similar in magnitude as values reported for runoff water in Sweden ($13.3 \mu\text{g L}^{-1}$; Bäckström et al. 2003). Cobalt is used in steel, paint, and as an additive in diesel (Makepeace et al. 1995; Roeva 1996), supporting the idea that Co is a good marker of traffic-related emission. Cadmium can be used for the manufacture of few components of motorized vehicles, such as brake pads and may reflect inputs by automobile use. However, during the event, the NBH collector site contributes few to daily Cd_d flux of the Jalle River (5%; Fig. 7), suggesting that other sources prevail.

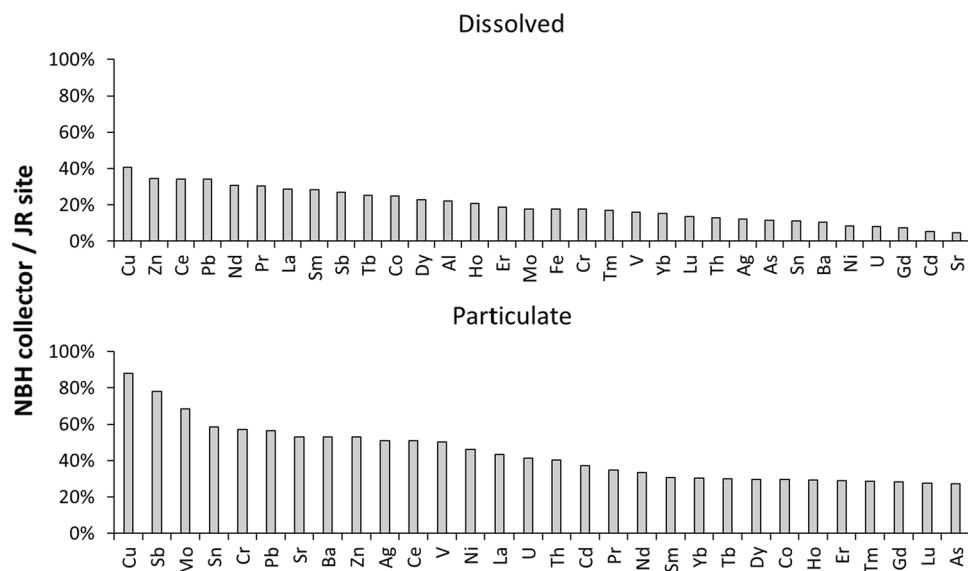
At the beginning and the end of the flood event on the Jalle River, the percentages of particulate REEs extracted by Aqua Regia were relatively low, i.e., ranging from 28% (Ce) to 75% (Tb) and from 39% (Ce) and 68% (Tb), compared with the samples showing the SPM peak. In fact, at 8:30 PM the percentages were $\sim 100\%$ whatever the REEs (Fig. 2). The REE content in the 8:30 PM sample from JR site obtained from selective extraction is roughly identical to that of the NBH collector site, supporting the idea that the particulate metals (classical trace metals and REEs) at the JR site come from the NBH collector.

The knowledge on the presence of traffic-emitted REEs in the environment is extremely limited, particularly for runoff waters. Lanthanum and Ce are more and more used as additives in the oil industry (Fluid catalytic cracking, Innocenzi et al. 2015; Krishnamurthy and Gupta 2015). Cerium also is used, along with the Platinum Group Metals (PGM) in catalytic converters (Montini et al. 2016; Wiseman et al. 2016). All of these metals are preferably used in the form of nanoparticles (Montini et al. 2016). If the signals of these elements during the event may be attributed to traffic-related sources, the low Gd (dissolved and particulate) contribution of the NBH collector to the Jalle River suggest that automotive activity is not responsible of the Gd anomalies observed at the JR site.

Period 3: Signals from Trace Metals Associated with the Upstream Watershed and/or WWTP

The third period covers samples 9–17 (9:30 PM–5:30 PM) showing high Cr_d and V_d concentrations associated with high/moderate water discharges (Fig. 6). These are the first samples after the NBH collector contribution period,

Fig. 7 Ratio of dissolved and particulate metal contributions with respect to NBH collector and Jalle River (JR site)



probably carrying signals from the upstream watershed. However, in this group, samples 15–17 (3:30 AM–5:30 AM) had the highest concentrations of Gd_d , Cd_d measured at the JR site throughout the rain event, as well as relatively high Ag_d concentrations (Fig. 6). This signal cannot be explained by the NBH collector supply but suggests urban wastewater inputs into the Jalle River, as Gd_d and Ag_d are known to be good tracers for urban wastewater. Several studies have related Gd_d anomalies in different aquatic systems to its use in medical structures (Hatje et al. 2016; Lerat-Hardy et al. 2019; Pereto et al. 2020; Song et al. 2017), as Gd serves as a contrast agent for MRI (Bau and Dulski 1996; Elbaz-Poulichet et al. 2002; Kulaksız and Bau 2011a). Furthermore, the normalized REE profile supports that the Gd_d peak at 4:30 AM is to 90% of anthropogenic origin. Silver is used by the medical industry, but also clothing and plastic industry, for its biocidal power (Blaser et al. 2008; Vance et al. 2015). The use of Cd is more ubiquitous, including (i) the manufacture of car batteries, and (ii) the manufacture of plastics, where it serves as a stabilizer (ATSDR 2012; Sahmoun et al. 2005). During the 4 h of the event, a WWTP located in the Jalle watershed upstream of the JR site discharged $\sim 2360 \text{ m}^3$ of treated wastewater but also had to bypass $\sim 3700 \text{ m}^3$ of untreated wastewater directly into the river. The WWTP contributed up to 46% of the discharge of the Jalle River during the bypass period, while during the low-water period (without storms) it contributed 32%. The bypass can be explained by the fact that the WWTP was no longer able to treat the wastewater directly or to store more wastewater for post-event treatment. Previous work on several influent and effluent samples ($n=6$) from this WWTP (REGARD project) has shown mean Cd_d and Ag_d concentrations of $0.194 \pm 0.27 \mu\text{g L}^{-1}$ and $0.038 \pm 0.018 \mu\text{g L}^{-1}$ in influent waters, respectively, and in effluent waters

the respective mean concentrations of Cd_d , Ag_d , and Gd_d were $0.146 \pm 0.201 \mu\text{g L}^{-1}$, $0.021 \pm 0.01 \mu\text{g L}^{-1}$, and $0.326 \pm 0.11 \mu\text{g L}^{-1}$.

Likewise, for influent waters, the mean concentrations of Cd_p and Ag_p are $0.033 \pm 0.038 \mu\text{g L}^{-1}$ and $0.080 \pm 0.048 \mu\text{g L}^{-1}$; for effluent waters, the mean concentration of Cd_p and Ag_p are $0.018 \pm 0.021 \mu\text{g L}^{-1}$ and $0.042 \pm 0.025 \mu\text{g L}^{-1}$. From these concentrations, the volume of treated wastewater discharged into the Jalle River and the volume of wastewater that has been bypassed, it is possible to estimate the dissolved and particulate metal fluxes from the WWTP. During the 4 h of the event, the dissolved Cd, Ag_d and Gd_d fluxes were respectively 1.06 g, 0.19 g, and 0.77 g. The particulate Cd and Ag_p fluxes are respectively 0.16 g and 0.40 g. The annual contribution per inhabitant to Cd_d reaching the WWTP is $0.002 \text{ g inhab}^{-1} \text{ yr}^{-1}$; this flux estimate is of the same order of magnitude than that of a previous study performed for main WWTPs of Bordeaux Metropole ($0.002 \text{ g inhab}^{-1} \text{ yr}^{-1}$; Deycard et al. 2014). Also, the annual Cd_p contribution per inhabitant ($0.001 \text{ g inhab}^{-1} \text{ yr}^{-1}$) of the Jalle River WWTP is of the same order of magnitude than that reported in the previous study ($0.001 \text{ g inhab}^{-1} \text{ yr}^{-1}$). Finally, the annual contributions per inhabitant of Ag_d ($0.001 \text{ g inhab}^{-1} \text{ yr}^{-1}$) and Ag_p ($0.003 \text{ g inhab}^{-1} \text{ yr}^{-1}$) of the Jalle River WWTP are lower than previously estimated for the main WWTPs of Bordeaux Metropole (Ag_d : $0.01 \text{ g inhab}^{-1} \text{ yr}^{-1}$ and Ag_p : $0.006 \text{ g inhab}^{-1} \text{ yr}^{-1}$; Deycard et al. 2017). This discrepancy may be due to the fact that, contrary to the Jalle River WWTP, the main Bordeaux Metropole WWTPs, located in the North and the South of the city, receive more wastewater from several hospitals.

The dissolved Cd and Cd_p fluxes estimated for the Jalle River WWTP were lower than that at the JR site

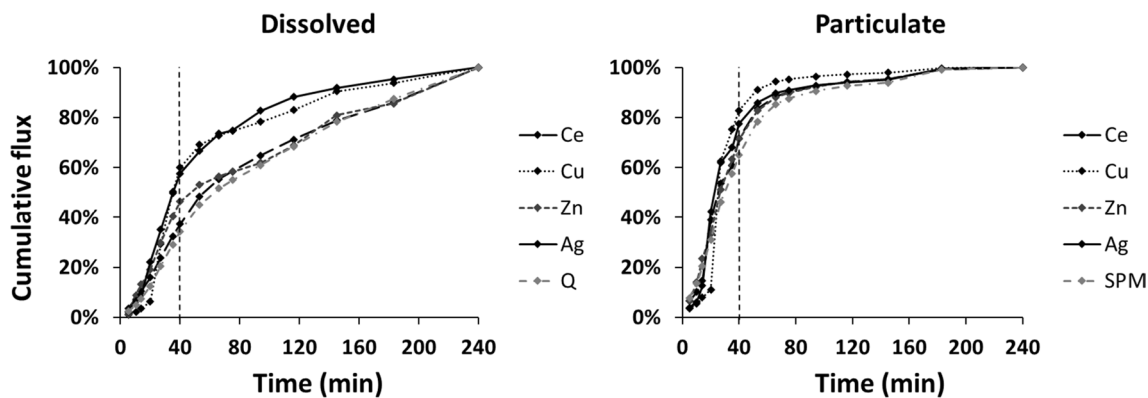


Fig. 8 Temporal variability of water discharge (Q), SPM, dissolved and particulate fluxes expressed by the relation between cumulative fluxes and time at the NBH collector site. Dashed lines represent 40 min (i.e., ~17% of time)

(Supplementary Data 3), suggesting that the WWTP contributes 8.3% of dissolved inputs and 0.8% of particulate inputs transported at the JR site, which implies the presence of additional source(s) (e.g., leaching of upstream agricultural soils on which phosphate fertilizers containing cadmium are applied). During the 4 h of the event, the WWTP contributed 37.1% of the Ag_d input to the Jalle River, making it a major source, whereas Ag_p flux in the WWTP was negligible, representing only 2.3% of that at the JR site (Supplementary Data 3). Finally, during the event, treated wastewater emitted by the WWTP contributed to 8.1% of Gd_d fluxes in the Jalle River (Supplementary Data 3), suggesting that the whole Gd_d flux might be roughly twofold greater, because there is no data on the Gd_d concentrations in the influent water. Therefore, it is impossible to estimate the bypass flux. It will be interesting to determine this value in the future.

Period 4: Influence of the Upstream Watershed

The fourth and last period includes the samples 18–24 (6:30 AM–12:30 PM) showing high values for Al_d , Fe_d , Ag_d , Th_d , As_d , Sm_d , Nd_d , Sb_d , Ce_d , La_d , and Pb_d (Fig. 6), interpreted as the geochemical signature of the upstream Jalle River watershed becoming dominant. Indeed, the pedology of the upstream part of the watershed is of the podzol type, which explains the increase of some metal concentrations, such as Al and Fe, as already observed in other systems (Viers et al. 2009). A better characterization of the influence of the watershed, according to the hydrological conditions, will have to be carried out.

Metal Contribution by Highway Runoff Water and Importance of the First Flush

Previous studies have developed formulae to determine the fluxes of dissolved and particulate metals exported per unit of road surface area and per year (Legret and Pagotto 1999;

Schueler 1987). These methods are frequently used in the scientific literature (Barrett et al. 1998; Prestes et al. 2006). However, they require the monitoring of several rainfall events. For the present study, these methods are not applicable because only one event was monitored. Although this major event most likely represents an important part of annual fluxes, these fluxes cannot be extrapolated to the annual scale as they probably are not representative of lower intensity rainfall events during the year.

In general, gross fluxes provide information on the overall element budget at a given site, whereas specific fluxes (gross element fluxes divided by watershed surface area) allow for a direct comparison between sites of the transport derived from different watershed areas. A summary of gross fluxes and specific fluxes for both sites (NBH collector and JR site) is presented in the Supplementary Data 3.

The estimated water and SPM flux from the NBH collector site was 23,200 m³ and 4900 kg during the 4 h monitoring, accounting respectively for ~15% and 60% of the daily SPM flux of the Jalle River (158,000 m³ and 8200 kg). The NBH collector metal contribution covers a wide range, depending on elements and partitioning, i.e., from 5% (Sr) to 40% (Cu) for the dissolved phase and from 30% (As) to 88% (Cu) for the particulate phase, note that the NBH collector site contribute to 78% for Sb_p (Fig. 7). The highest dissolved and particulate metal contributions are not only due to water and SPM contribution, suggesting that water and particles are enriched in these metals compared with the Jalle River, especially for dissolved and particulate Cu, Sb_p and Zn_d , Ce_d , and Pb_d .

The temporal variability of dissolved and particulate metal fluxes in the NBH collector is highlighted by the cumulated dissolved and particulate metal fluxes, expressed as the percent of metal fluxes over the time in combination with water flux for the dissolved phase and SPM flux for the particulate phase (Fig. 8). The first 40 min of the event (i.e., <17% of time) contributed 35% of the water discharge

exported by the NBH collector, transporting 32–63% of the dissolved metals load (Fig. 8). The same time span represented ~65% of both the total SPM flux and associated particulate metals, highlighting the importance of monitoring the first minutes of rainy events, even if the first flush does not necessarily correspond to the maximum water discharge.

Conception of a Highway Runoff Water Treatment Plant

The functioning of recent sewage networks is currently based on separate networks, i.e., networks separating domestic wastewater from surface runoff. In this case, runoff water is generally discharged without treatment (or after minimum treatment to reduce the particulate phase) into the aquatic environment, raising the problem of dispersing metals and other contaminants. An “in-pipe” treatment may be necessary to limit metal fluxes spilled at the outlet of the separate network. In the framework of the REGARD project, a technology for the treatment of micropollutants in runoff before emission into the Jalle River was implemented by means of a demonstration plant pilot on a derivation of the NBH collector (Salsnes®; Jansen 2016). This technology relied on a coupled rotating-belt filtration based using injection of reagents: three with anionic coagulant and flocculant (SNF EM630) and one with cationic flocculant (SNF EM 840 CT).

Several factors need to be considered to treat highway runoff so that it does not have a negative impact on surface water (Huber et al. 2016). It is important adjust the treatment to the different main carrier phases. Considering that particles are the dominant carrier phase, it appears necessary to set up a filtration and/or decantation system to limit metal exports. Particulate metals are eliminated up to 80% in the presence of reagents (coagulation/flocculation or flocculation alone). The decrease of pollution is directly correlated to the SPM decrease by the demonstration plant pilot. Thus, the impact of the demonstration plant pilot, to reduce the pollution, become lower in the case lower SPM concentrations.

However, some metals have important dissolved fluxes (e.g., Cu and Zn). Based on the results obtained with the demonstration plant pilot, dissolved metals are not eliminated from waters even in the presence of reagents. Concentration of certain metals, such as Co_d , Zn_d , and Ni_d , were even greater after the treatment than before, probably due to impurities provided by the coagulant. It is therefore useful to set up another treatment device to reduce dissolved metal fluxes (Kayhanian et al. 2012), such as the use of membrane filtration, a technology that is already used in WWTPs (Fu and Wang 2011).

High-frequency monitoring at the NBH collector site has shown that most of metal fluxes are carried by the first flush waters. However, it is still necessary to treat all runoff waters

for several reasons (Flint and Davis 2007; Maniquiz-Redillas and Kim 2014): (i) it is possible that a second flush of heavily contaminated waters occurs depending the size and/or morphology of the watershed and/or the specificity of the highway sites; and (ii) although a relationship exists between metal concentrations and the intensity of the rainy event (Crabtree et al. 2006; Kang et al. 2008; Pitt et al. 1995), not all the metals attached to the highway surfaces may be mobilized by the first rainy event following a dry weather period (Cristina and Sansalone 2003). Joint Research and Development involving both the scientific community and managers is necessary to develop an efficient technology to treat different runoff waters and particularly those of the first flush.

Conclusions

At the end of this work, several points can be concluded: (i) the urban highways are nonnegligible sources for a variety of metals and their runoff can affect aquatic ecosystems, especially the first flush waters; (ii) emerging metals, such as Ce, appear to be good tracers for automotive activities; and (iii) the partitioning of trace metals in the present work suggests that the treatment of runoff waters should cover both the particulate and the dissolved phase.

Climate change tends to impact precipitation patterns with increasing periods of low river water (and consequently weaker dilution of contaminants) and changes in the occurrence of rainy/flood events that may serve as main contaminant vectors. It is therefore important to precisely quantify metal fluxes resulting from automobile activity during rainy episodes to (i) better understand their potential impact on aquatic ecosystems, (ii) develop efficient runoff treatment strategies for both historically used metals and those of emerging concern due to recent high-tech applications, and (iii) aim to recycle rare and/or precious metals for which there is growing demand and a risk of shortage (the so-called Technology Critical Elements; e.g., PGM, REEs).

Supplementary Information The online version of this article (<https://doi.org/10.1007/s00244-021-00816-4>) contains supplementary material, which is available to authorized users.

Acknowledgements This work has been supported by the Regional Water Agency (Agence de l’Eau Adour-Garonne) and the “Agence Française pour la Biodiversité” in the frame of the REGARD Project: “Comprehensive and integrated programme against micropollutants (Bordeaux-Métropole).” The authors thank Bruno Barillon and Ywann Penru (CIRSEE) for managing the demonstration plant pilot and Lionel Dutruch for his analytical assistance. The analyses were performed by the instrumental platform “Majeurs et Métaux traces” (M&Ms, EPOC, University of Bordeaux). The author Antoine Lerat-Hardy has benefited from a PhD grant by the French Ministry of “Enseignement Supérieur, de la Recherche et de l’Innovation.”

Author Contributions Antoine LERAT-HARDY (Writing—original draft; Data curation; Conceptualization), Alexandra COYNEL (Writing—original draft; Supervision, Conceptualization, Investigation), Jörg SCHÄFER (Writing—review & editing, Validation), Antoine MARACHE (Writing—review & editing; Formal Analysis), Clément PERETO (Writing—review & editing), Cécile BOSSY (Writing—review & editing), Marion-Justine CAPDEVILLE (Writing—review & editing, Investigation), Damien GRANGER (Writing—review & editing, Investigation).

Funding This work has been supported by the Regional Water Agency (Agence de l’Eau Adour-Garonne) and the “Agence Française pour la Biodiversité” in the frame of the REGARD Project: “Comprehensive and integrated programme against micropollutants (Bordeaux-Métropole).” The authors Antoine Lerat-Hardy has benefited from a PhD grant by the French Ministry of “Enseignement Supérieur, de la Recherche et de l’Innovation”.

Compliance with Ethical Standards

Conflicts of Interest The authors declare that they have no conflict of interest.

Availability of Data and Material The datasets generated during and/or analysed during the current study are available from the corresponding author on reasonable request.

References

- Abdou M et al (2016) Past and present platinum contamination of a major European fluvial–estuarine system: Insights from river sediments and estuarine oysters. *Mar Chem* 185:104–110. <https://doi.org/10.1016/j.marchem.2016.01.006>
- Arrouays D, Wilbert J, Richer-De-Forges A (2015) Référentiel Régional Pédologique d’Aquitaine. Carte des pédopaysages des départements des Landes et de la Gironde (Etude n°30111). INRAE
- ATSDR (2012) Toxicological profile for Cadmium. U.S. Department of Health and Human Services, Public Health Service, Atlanta, GA
- Bäckström M, Nilsson U, Håkansson K, Allard B, Karlsson S (2003) Speciation of heavy metals in road runoff and roadside total deposition. *Water Air Soil Pollut* 147:343–366. <https://doi.org/10.1023/a:1024545916834>
- Ball JE (2002) Stormwater quality at Centennial Park, Sydney, Australia. University of New South Wales, Department of Civil and Environmental
- Ball JE, Jenks R, Aubourg D (1998) An assessment of the availability of pollutant constituents on road surfaces. *Sci Total Environ* 209:243–254. [https://doi.org/10.1016/S0048-9697\(98\)80115-0](https://doi.org/10.1016/S0048-9697(98)80115-0)
- Bannerman RT, Owens DW, Dodds RB, Hornewer NJ (1993) Sources of pollutants in Wisconsin stormwater. *Water Sci Technol* 28:241–259
- Barrett ME, Irish LB, Malina JF, Charbeneau RJ (1998) Characterization of highway runoff in Austin, Texas, area. *J Environ Eng* 124:131–137. [https://doi.org/10.1061/\(asce\)0733-9372\(1998\)124:2\(131\)](https://doi.org/10.1061/(asce)0733-9372(1998)124:2(131))
- Bau M, Dulski P (1996) Anthropogenic origin of positive gadolinium anomalies in river waters. *Earth Planetary Sci Lett* 143:245–255. [https://doi.org/10.1016/0012-821X\(96\)00127-6](https://doi.org/10.1016/0012-821X(96)00127-6)
- Bau M, Schmidt K, Pack A, Bendel V, Kraemer D (2018) The European Shale: an improved data set for normalisation of rare earth element and yttrium concentrations in environmental and biological samples from Europe. *Appl Geochem* 90:142–149. <https://doi.org/10.1016/j.apgeochem.2018.01.008>
- Berbee R, Rijs G, De Brouwer R (1999) Characterization and treatment of runoff from highways in the Netherlands paved with impervious and pervious asphalt. *Water Environ Res* 71:183–190
- Blaser SA, Scheringer M, MacLeod M, Hungerbühler K (2008) Estimation of cumulative aquatic exposure and risk due to silver: Contribution of nano-functionalized plastics and textiles. *Sci Total Environ* 390:396–409. <https://doi.org/10.1016/j.scitotenv.2007.10.010>
- Brauer (2015) Top 10 advanced car technologies by 2020. *Forbes*
- Cobelo-García A et al (2015) COST action TD1407: network on technology-critical elements (NOTICE)—from environmental processes to human health threats. *Environ Sci Pollut Res* 22:15188–15194. <https://doi.org/10.1007/s11356-015-5221-0>
- Coynel A et al (2016) Spatial distribution of trace elements in the surface sediments of a major European estuary (Loire Estuary, France): source identification and evaluation of anthropogenic contribution. *J Sea Res* 118:77–91. <https://doi.org/10.1016/j.seares.2016.08.005>
- Coynel A, Schäfer J, Blanc G, Bossy C (2007) Scenario of particulate trace metal and metalloids transport during a major flood event inferred from transient geochemical signals. *Appl Geochem* 22:821–836. <https://doi.org/10.1016/j.apgeochem.2006.10.004>
- Crabtree B, Moy F, Whitehead M, Roe A (2006) Monitoring pollutants in highway runoff. *Water Environ J* 20:287–294. <https://doi.org/10.1111/j.1747-6593.2006.00033.x>
- Cristina CM, Sansalone JJ (2003) First flush, power law and particle separation diagrams for urban storm-water suspended particulates. *J Environ Eng* 129:298–307. [https://doi.org/10.1061/\(ASCE\)0733-9372\(2003\)129:4\(298\)](https://doi.org/10.1061/(ASCE)0733-9372(2003)129:4(298))
- Davis AP, Shokouhian M, Ni S (2001) Loading estimates of lead, copper, cadmium, and zinc in urban runoff from specific sources. *Chemosphere* 44:997–1009. [https://doi.org/10.1016/S0045-6535\(00\)00561-0](https://doi.org/10.1016/S0045-6535(00)00561-0)
- Deycard VN et al (2014) Contributions and potential impacts of seven priority substances (As, Cd, Cu, Cr, Ni, Pb, and Zn) to a major European Estuary (Gironde Estuary, France) from urban wastewater. *Mar Chem* 167:123–134. <https://doi.org/10.1016/j.marchem.2014.05.005>
- Deycard VN et al (2017) Inputs, dynamics and potential impacts of silver (Ag) from urban wastewater to a highly turbid estuary (SW France). *Chemosphere* 167:501–511. <https://doi.org/10.1016/j.chemosphere.2016.09.154>
- Dierkes C, Geiger WF (1998) Decontaminating effect of greened highway embankments. In: Proceedings of the NOVATECH-Conference, Lyon, France, 1998. Citeseer, p 4–6
- Elbaz-Poulichet F, Seidel J-L, Othoniel C (2002) Occurrence of an anthropogenic gadolinium anomaly in river and coastal waters of Southern France. *Water Res* 36:1102–1105. [https://doi.org/10.1016/S0043-1354\(01\)00370-0](https://doi.org/10.1016/S0043-1354(01)00370-0)
- Ellis JB, Revitt DM (1982) Incidence of heavy metals in street surface sediments: Solubility and grain size studies. *Water Air Soil Pollut* 17:87–100. <https://doi.org/10.1007/bf00164094>
- Eriksson E et al (2007) Selected stormwater priority pollutants—a European perspective. *Sci Total Environ* 383:41–51. <https://doi.org/10.1016/j.scitotenv.2007.05.028>
- Flint KR, Davis AP (2007) Pollutant mass flushing characterization of highway stormwater runoff from an ultra-urban area. *J Environ Eng* 133:616–626. [https://doi.org/10.1061/\(ASCE\)0733-9372\(2007\)133:6\(616\)](https://doi.org/10.1061/(ASCE)0733-9372(2007)133:6(616))
- Fu F, Wang Q (2011) Removal of heavy metal ions from wastewaters: a review. *J Environ Manag* 92:407–418. <https://doi.org/10.1016/j.jenvman.2010.11.011>
- Fujiwara F, Rebagliati RJ, Marrero J, Gómez D, Smichowski P (2011) Antimony as a traffic-related element in size-fractionated road

- dust samples collected in Buenos Aires. *Microchem J* 97:62–67. <https://doi.org/10.1016/j.microc.2010.05.006>
- Furumai H, Balmer H, Boller M (2002) Dynamic behavior of suspended pollutants and particle size distribution in highway runoff. *Water Sci Technol* 46:413–418. <https://doi.org/10.2166/wst.2002.0771>
- Gil-Díaz T, Schäfer J, Coynel A, Bossy C, Dutruch L, Blanc G (2018) Antimony in the Lot-Garonne river system: a 14-year record of solid–liquid partitioning and fluxes. *Environ Chem* 15:121–136. <https://doi.org/10.1071/EN17188>
- Han Y, Lau S-L, Kayhanian M, Stenstrom MK (2006) Characteristics of highway stormwater runoff. *Water Environ Res* 78:2377–2388. <https://doi.org/10.2175/106143006X95447>
- Hatje V, Bruland KW, Flegal AR (2016) Increases in anthropogenic gadolinium anomalies and rare earth element concentrations in San Francisco Bay over a 20-year record. *Environ Sci Technol* 50:4159–4168. <https://doi.org/10.1021/acs.est.5b04322>
- Hocquard C (2011) Les matières premières comme enjeu stratégiques majeur : le cas des terres rares. Paper presented at the 23e Rendez-vous de la Mondialisation Matières premières, métaux rares, ressources énergétiques: quel impact de la mondialisation, Paris
- Huber M, Welker A, Helmreich B (2016) Critical review of heavy metal pollution of traffic area runoff: occurrence, influencing factors, and partitioning. *Sci Total Environ* 541:895–919. <https://doi.org/10.1016/j.scitotenv.2015.09.033>
- Innocenzi V, Ferella F, De Michelis I, Vegliò F (2015) Treatment of fluid catalytic cracking spent catalysts to recover lanthanum and cerium: comparison between selective precipitation and solvent extraction. *J Ind Eng Chem* 24:92–97. <https://doi.org/10.1016/j.jiec.2014.09.014>
- IUPAC (1971) Nomenclature of inorganic chemistry; definitive rules 1970. Butterworths, London
- Jansen R (2016) Successful pilot test of rotating belt filters. *Filtr Sep* 53:26–27. [https://doi.org/10.1016/S0015-1882\(16\)30165-3](https://doi.org/10.1016/S0015-1882(16)30165-3)
- Kang J-H, Kayhanian M, Stenstrom MK (2008) Predicting the existence of stormwater first flush from the time of concentration. *Water Res* 42:220–228. <https://doi.org/10.1016/j.watres.2007.07.001>
- Kayhanian M (2012) Trend and concentrations of legacy lead (Pb) in highway runoff. *Environ Pollut* 160:169–177. <https://doi.org/10.1016/j.envpol.2011.09.009>
- Kayhanian M, Fruchtmann BD, Gulliver JS, Montanaro C, Ranieri E, Wuertz S (2012) Review of highway runoff characteristics: comparative analysis and universal implications. *Water Res* 46:6609–6624. <https://doi.org/10.1016/j.watres.2012.07.026>
- Kayhanian M, Stransky C, Bay S, Lau SL, Stenstrom MK (2008) Toxicity of urban highway runoff with respect to storm duration. *Sci Total Environ* 389:386–406. <https://doi.org/10.1016/j.scitotenv.2007.08.052>
- Kayhanian M, Suverkropp C, Ruby A, Tsay K (2007) Characterization and prediction of highway runoff constituent event mean concentration. *J Environ Manag* 85:279–295. <https://doi.org/10.1016/j.jenvman.2006.09.024>
- Kim L-H, Kayhanian M, Lau S-L, Stenstrom MK (2005) A new modeling approach for estimating first flush metal mass loading. *Water Sci Technol* 51:159–167. <https://doi.org/10.2166/wst.2005.0587>
- Kim L-H, Zoh K-D, Jeong S-m, Kayhanian M, Stenstrom MK (2006) Estimating pollutant mass accumulation on highways during dry periods. *J Environ Eng* 132:985–993. [https://doi.org/10.1061/\(ASCE\)0733-9372\(2006\)132:9\(985\)](https://doi.org/10.1061/(ASCE)0733-9372(2006)132:9(985))
- Krishnamurthy N, Gupta CK (2015) Extractive metallurgy of rare earths. CRC Press, Boca Raton
- Kulaksız S, Bau M (2011a) Anthropogenic gadolinium as a microcontaminant in tap water used as drinking water in urban areas and megacities. *Appl Geochem* 26:1877–1885. <https://doi.org/10.1016/j.apgeochem.2011.06.011>
- Kulaksız S, Bau M (2011b) Rare earth elements in the Rhine River, Germany: first case of anthropogenic lanthanum as a dissolved microcontaminant in the hydrosphere. *Environ Int* 37:973–979. <https://doi.org/10.1016/j.envint.2011.02.018>
- Lau S-L, Han Y, Kang J-H, Kayhanian M, Stenstrom MK (2009) Characteristics of highway stormwater runoff in Los Angeles: metals and polycyclic aromatic hydrocarbons. *Water Environ Res* 81:308–318. <https://doi.org/10.2175/106143008X357237>
- Lee H, Lau S-L, Kayhanian M, Stenstrom MK (2004) Seasonal first flush phenomenon of urban stormwater discharges. *Water Res* 38:4153–4163. <https://doi.org/10.1016/j.watres.2004.07.012>
- Legret M, Pagotto C (1999) Evaluation of pollutant loadings in the runoff waters from a major rural highway. *Sci Total Environ* 235:143–150. [https://doi.org/10.1016/S0048-9697\(99\)00207-7](https://doi.org/10.1016/S0048-9697(99)00207-7)
- Lerat-Hardy A et al (2019) Rare Earth Element fluxes over 15 years into a major European Estuary (Garonne-Gironde, SW France): hospital effluents as a source of increasing gadolinium anomalies. *Sci Total Environ* 656:409–420. <https://doi.org/10.1016/j.scitotenv.2018.11.343>
- Li Y, Kang J-H, Lau S-L, Kayhanian M, Stenstrom MK (2008) Optimization of settling tank design to remove particles and metals. *J Environ Eng* 134:885–894. [https://doi.org/10.1061/\(ASCE\)0733-9372\(2008\)134:11\(885\)](https://doi.org/10.1061/(ASCE)0733-9372(2008)134:11(885))
- Li Y, Lau S-L, Kayhanian M, Stenstrom MK (2005) Particle size distribution in highway runoff. *J Environ Eng* 131:1267–1276. [https://doi.org/10.1061/\(ASCE\)0733-9372\(2005\)131:9\(1267\)](https://doi.org/10.1061/(ASCE)0733-9372(2005)131:9(1267))
- Li Y, Lau S-L, Kayhanian M, Stenstrom MK (2006) Dynamic characteristics of particle size distribution in highway runoff: implications for settling tank design. *J Environ Eng* 132:852–861. [https://doi.org/10.1061/\(ASCE\)0733-9372\(2006\)132:8\(852\)](https://doi.org/10.1061/(ASCE)0733-9372(2006)132:8(852))
- Makepeace DK, Smith DW, Stanley SJ (1995) Urban stormwater quality: summary of contaminant data. *Crit Rev Environ Sci Technol* 25:93–139. <https://doi.org/10.1080/10643389509388476>
- Mangani G, Berloni A, Bellucci F, Tatano F, Maione M (2005) Evaluation of the pollutant content in road runoff first flush waters. *Water Air Soil Pollut* 160:213–228
- Maniquiz-Redillas M, Kim L-H (2014) Fractionation of heavy metals in runoff and discharge of a stormwater management system and its implications for treatment. *J Environ Sci* 26:1214–1222. [https://doi.org/10.1016/S1001-0742\(13\)60591-4](https://doi.org/10.1016/S1001-0742(13)60591-4)
- Marks M, Mason J, Oliveira G (2016) People near transit: improving accessibility and rapid transit coverage in large cities. Institute for Transportation & Development Policy
- Martínez LLG, Poletto C (2014) Assessment of diffuse pollution associated with metals in urban sediments using the geoaccumulation index (Igeo). *J Soils Sediments* 14:1251–1257. <https://doi.org/10.1007/s11368-014-0871-y>
- McKenzie ER, Money JE, Green PG, Young TM (2009) Metals associated with stormwater-relevant brake and tire samples. *Sci Total Environ* 407:5855–5860. <https://doi.org/10.1016/j.scitotenv.2009.07.018>
- Météo France (2019) Données climatiques de la station de Bordeaux. <http://www.meteofrance.com/climat/france/bordeaux/33281001/normales>
- Montini T, Melchionna M, Monai M, Fornasiero P (2016) Fundamentals and catalytic applications of CeO₂-based materials. *Chem Rev* 116:5987–6041. <https://doi.org/10.1021/acs.chemrev.5b00603>
- Padoan E, Ajmone-Marsan F, Querol X, Amato F (2018) An empirical model to predict road dust emissions based on pavement and traffic characteristics. *Environ Pollut* 237:713–720. <https://doi.org/10.1016/j.envpol.2017.10.115>
- Pereto C, Coynel A, Lerat-Hardy A, Gourves P-Y, Schäfer J, Baudrimont M (2020) Corbicula fluminea: a sentinel species for urban rare earth element origin. *Sci Total Environ*. <https://doi.org/10.1016/j.scitotenv.2020.138552>

- Pitt R, Field R, Lalor M, Brown M (1995) Urban stormwater toxic pollutants: assessment, sources, and treatability. *Water Environ Res* 67:260–275. <https://doi.org/10.2175/106143095x131466>
- Prestes EC, Anjos VED, Sodré FF, Grassi MT (2006) Copper, lead and cadmium loads and behavior in urban stormwater runoff in Curitiba, Brazil. *J Braz Chem Soc* 17:53–60. <https://doi.org/10.1590/s0103-50532006000100008>
- Roeva N (1996) Special features of the behavior of heavy metals in various natural environments. *J Anal Chem* 51:352–364
- Sahmoun AE, Case LD, Jackson SA, Schwartz GG (2005) Cadmium and prostate cancer: a critical epidemiologic analysis. *Cancer Invest* 23:256–263. <https://doi.org/10.1081/CNV-200055968>
- Sansalone JJ, Buchberger SG (1997) Partitioning and first flush of metals in urban roadway storm water. *J Environ Eng* 123:134–143. [https://doi.org/10.1061/\(ASCE\)0733-9372\(1997\)123:2\(134\)](https://doi.org/10.1061/(ASCE)0733-9372(1997)123:2(134))
- Schäfer J, Puchelt H (1998) Platinum-Group-Metals (PGM) emitted from automobile catalytic converters and their distribution in roadside soils. *J Geochem Expl* 64:307–314
- Schueler TR (1987) Controlling urban runoff: a practical manual for planning and designing urban BMPs. Department of Environmental Programs, Metropolitan Washington Council of Governments, Washington, D.C.
- Shelley PE, Driscoll ED, Sartor JD (1987) Probabilistic characterization of pollutant discharges from highway stormwater runoff. *Sci Total Environ* 59:401–410. [https://doi.org/10.1016/0048-9697\(87\)90463-3](https://doi.org/10.1016/0048-9697(87)90463-3)
- Shi G, Chen Z, Bi C, Li Y, Teng J, Wang L, Xu S (2010) Comprehensive assessment of toxic metals in urban and suburban street deposited sediments (SDSs) in the biggest metropolitan area of China. *Environ Pollut* 158:694–703. <https://doi.org/10.1016/j.envpol.2009.10.020>
- Sholkovitz ER (1992) Chemical evolution of rare earth elements: fractionation between colloidal and solution phases of filtered river water. *Earth Planet Sci Lett* 114:77–84. [https://doi.org/10.1016/0012-821X\(92\)90152-L](https://doi.org/10.1016/0012-821X(92)90152-L)
- Sholkovitz ER (1995) The aquatic chemistry of rare earth elements in rivers and estuaries. *Aquat Geochem* 1:1–34. <https://doi.org/10.1007/BF01025229>
- Smullen JT, Shallcross AL, Cave KA (1999) Updating the U.S. Nationwide urban runoff quality data base. *Water Sci Technol* 39:9–16. [https://doi.org/10.1016/S0273-1223\(99\)00312-1](https://doi.org/10.1016/S0273-1223(99)00312-1)
- Song H, Shin W-J, Ryu J-S, Shin HS, Chung H, Lee K-S (2017) Anthropogenic rare earth elements and their spatial distributions in the Han River, South Korea. *Chemosphere* 172:155–165. <https://doi.org/10.1016/j.chemosphere.2016.12.135>
- Sternbeck J, Sjödin Å, Andréasson K (2002) Metal emissions from road traffic and the influence of resuspension—results from two tunnel studies. *Atmos Environ* 36:4735–4744. [https://doi.org/10.1016/S1352-2310\(02\)00561-7](https://doi.org/10.1016/S1352-2310(02)00561-7)
- Vance ME, Kuiken T, Vejerano EP, McGinnis SP, Hochella MF Jr, Rejeski D, Hull MS (2015) Nanotechnology in the real world: redeveloping the nanomaterial consumer products inventory. *Beilstein J Nanotechnol* 6:1769–1780. <https://doi.org/10.3762/bjnano.6.181>
- Viers J, Dupré B, Gaillardet J (2009) Chemical composition of suspended sediments in World Rivers: new insights from a new database. *Sci Total Environ* 407:853–868. <https://doi.org/10.1016/j.scitotenv.2008.09.053>
- von Uexküll O, Skerfving S, Doyle R, Braungart M (2005) Antimony in brake pads—a carcinogenic component? *J Cleaner Product* 13:19–31. <https://doi.org/10.1016/j.jclepro.2003.10.008>
- Westerlund C, Viklander M (2006) Particles and associated metals in road runoff during snowmelt and rainfall. *Sci Total Environ* 362:143–156. <https://doi.org/10.1016/j.scitotenv.2005.06.031>
- Wilson D (2006) Highway 520 bridge stormwater runoff study. King County Water and Land Resources Division, Department of Natural Resources and Parks
- Wiseman CLS, Hassan Pour Z, Zereini F (2016) Platinum group element and cerium concentrations in roadside environments in Toronto, Canada. *Chemosphere* 145:61–67. <https://doi.org/10.1016/j.chemosphere.2015.11.056>
- Yousef YA, Wanielista MP, Hvitved-Jacobsen T, Harper HH (1984) Fate of heavy metals in stormwater runoff from highway bridges. *Sci Total Environ* 33:233–244. [https://doi.org/10.1016/0048-9697\(84\)90397-8](https://doi.org/10.1016/0048-9697(84)90397-8)